An Investigation of Helicopter Rotor Blade Flap Vibratory Loads

William G. Bousman and Thomas H. Maier
Research Scientists
U.S. Army Aeroflightdynamics Directorate (AVSCOM)
Moffett Field, California 94035

ABSTRACT

The analysis CAMRAD/JA is used to model two aircraft, a Puma with a swept-tip blade, and a UH–60A Black Hawk. The accuracy of the analysis to predict the blade vibratory flap bending moments is assessed by comparing the predicted moments with measurements from flight test. The influence of assumptions in the analytical model is examined by varying model parameters, reducing the degrees of freedom, and so forth and comparing the predicted results to baseline values for the vibratory loads. In general, the analysis underpredicts the 3/rev and 4/rev flap bending moments in the blade, both at low and high speeds. The qualitative prediction of the loads, however, is quite good for the research Puma, but less satisfactory for the Black Hawk. The examination of modeling assumptions demonstrates the importance of the vortex wake at low speed and the importance of the airload distribution dictated by roll moment balance at high speed.

INTRODUCTION

The calculation of helicopter vibratory loads remains a difficult problem. The satisfactory prediction of vibration requires a correct calculation of the forces and moments on the blade, the aeroelastic response of the blade to these forces and moments, the vibratory forces and moments transmitted to the hub, and the response of the helicopter fuselage to the vibratory loads. Each of the elements of this calculation is affected by the other elements and all of the connections between the various parts of the problem must be considered.

Reference 1 has compared structural measurements from flight test or wind tunnel test for a number of helicopter rotors. The purpose of that comparison was to identify those vibratory loads characteristics that are common to a number of aircraft and, in this sense, are representative of the fundamental physics of the rotor vibratory loads problem. Common characteristics were noted for the flap vibratory loads, the torsional vibratory loads, and, to a lesser degree, the chord vibratory loads. It was concluded that these common or similar load behaviors provide a good test for theoretical methods. In particular, it seems likely that a theoretical method will only be successful when it can demonstrate that it reproduces the common or similar characteristics for a variety of different rotors or aircraft.

In a recent comparison of four analytical methods with flight test data obtained from a research Puma,[2] it was concluded that the best of these analytical methods show reasonable predictions of the flap vibratory loading at high speed although the prediction of the low-speed vibratory loads was less successful. The prediction of the chord and torsional vibratory loads, on the other hand, was poor. These results are sufficiently good to encourage further comparison of the analytical methods with experimental measurements for flap vibratory loading and the continuation of this work is the general focus of this paper.

The basic behavior of the flap vibratory load problem is illustrated in Figures 1 and 2 where nondimensional flap bending moments from two helicopters are compared over a range of advance ratio, μ. The nondimensionalization is based on blade loading, rather than response, that is,

$$\frac{C_{FM}}{\sigma} = \frac{M_F}{\rho b c \Omega^2 R^4}$$

where σ is the rotor solidity, M_F the flap bending moment, ρ the air density, b the number of blades, c the blade chord, Ω the rotor speed, and R the blade radius.

Both of these rotors have four blades and, therefore, the 3/rev and 4/rev loads have the greatest impact on vibration. The 3/rev flap bending moments in the blade are the primary source of the 4/rev pitch and roll hub moments (the 5/rev blade loads are often considerably smaller than the 3/rev loads) and the 4/rev flap loads are the source of the 4/rev vertical hub shears. The qualitative behavior of both

Presented at the 48th Annual Forum of the American Helicopter Society, Washington, D.C., June 1992.

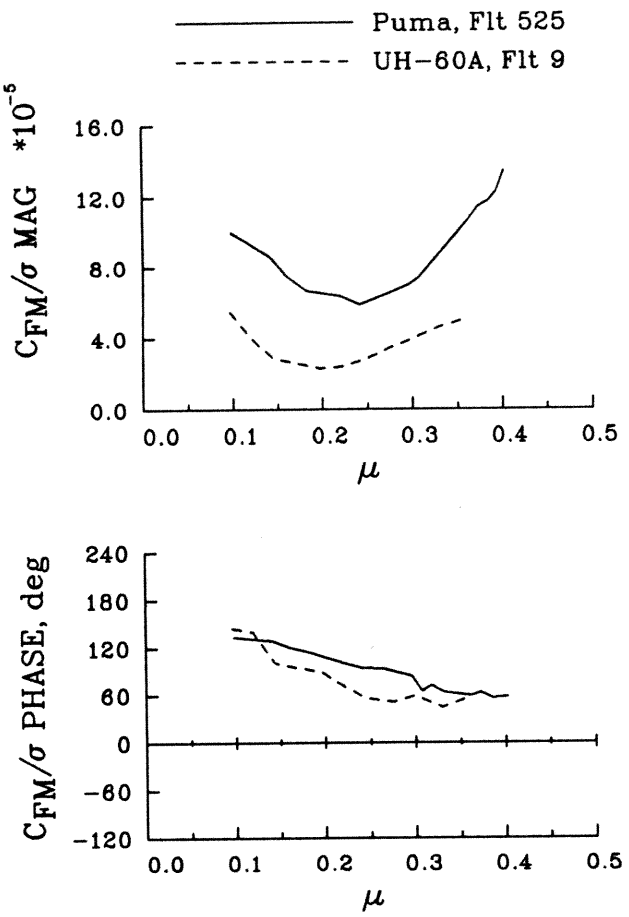

Figure 1. – 3/Rev flap bending moments as a function of advance ratio; research Puma, Flight 525, $C_T/\sigma = 0.070$, $r/R = 0.57$; UH–60A, Flight 9, $C_T/\sigma = 0.080$, $r/R = 0.50$.

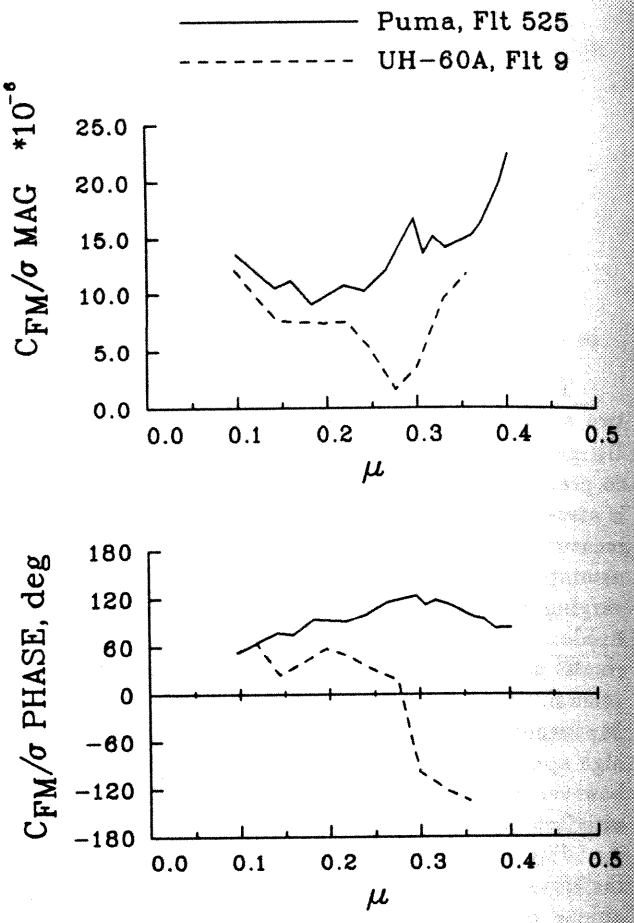

Figure 2. – 4/Rev flap bending moments as a function of advance ratio; research Puma, Flight 525, $C_T/\sigma = 0.070$, $r/R = 0.67$; UH–60A, Flight 9, $C_T/\sigma = 0.080$, $r/R = 0.70$.

rotors is similar at 3/rev and these similarities have been noted previously for other rotors.[1] However, the 4/rev qualitative behavior of the two rotors is different and there are quantitative differences in the response amplitude at both 3/rev and 4/rev. The test of an analytical method in this case, then, is to first match the qualitative behavior of the loading and second match the amplitude of the load. The CAMRAD/JA analysis[3] will be used for these comparisons. The purpose of this paper, then, is to evaluate the capability of the CAMRAD/JA analysis to predict the flap vibratory loading of these two rotors and, through this evaluation, better understand what improvements are needed in analytical methods to enable the correct prediction of vibratory loads.

FLIGHT TEST DATA

The research Puma data used here are part of a large data base obtained over a number of years at the Defence Research Agency (DRA) in Bedford (formerly the Royal Aerospace Establishment).[2] The data were obtained under a joint Anglo-French program and have not been published. The blade used on the research Puma is illustrated in Figure 3. The rectangular tip of the standard Puma blade has been modified to provide the tip planform shown in the figure. Absolute pressures were measured on the upper and lower surfaces of the modified section at $0.92R$, $0.95R$, and $0.978R$ and upper surface pressures only at $0.89R$. Flap bending moment measurements were obtained at eleven stations from the blade shank outboard as indicated in the figure. A single revolution of data was taken for each flight test point, therefore, there

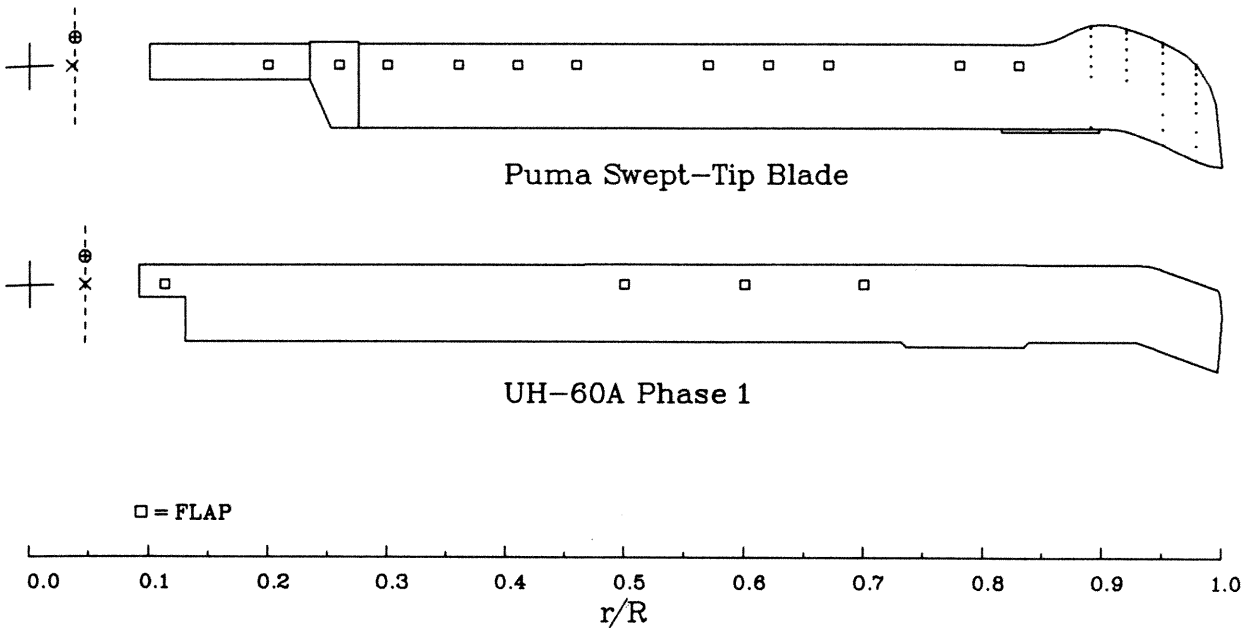

Figure 3. – Research Puma and UH–60A blade planforms. Pressure arrays shown by dots (Puma only) and flap bending moment bridges by open squares.

is no averaging of the data. The data were sampled at 256 points over each revolution which provides a bandwidth of 128 harmonics (azimuthal resolution of 1.4°).

The UH–60A data used here were obtained in a NASA/Army test in 1987[4] and are stored in an electronic data base. The blade tested is illustrated in Figure 3 and is identical to the standard UH–60A blade. The blade was instrumented with four flap bending moment bridges as indicated in the figure. No pressure instrumentation was installed for these tests. Approximately five seconds of data were obtained at each test point and a 20-cycle average has been used for the results shown here. The bandwidth of 128 harmonics is the same as obtained on the research Puma.

FLAP BENDING MOMENT CORRELATION

Aircraft Trim

The research Puma was modeled in CAMRAD/JA as a single isolated rotor. The rotor trim was specified by setting the flight speed, the rotor thrust, the shaft angle, and the first harmonic flapping based on flight test measurements. The trim procedure and comparisons of calculation and measurement for unspecified trim parameters are discussed in Appendix 1.

The UH–60A was modeled as an aircraft with a single main rotor and a single tail rotor for antitorque. Rotor trim was specified by setting the flight speed and requiring that the aircraft forces and moments be balanced for zero sideslip conditions. This trim procedure and comparisons of calculation and measurements for unspecified trim parameters are discussed in Appendix 2.

Vibratory Flap Bending Moments

The measured vibratory flap bending moments at midspan, harmonics 3 and above, for the research Puma and the UH–60A are compared in Figures 4 and 5 with the CAMRAD/JA analysis using the free wake option. The nondimensional bending moment is shown as a function of the blade azimuth and the advance ratio. The vibratory loading at this span location is dominated by the 3/rev component of the load. The qualitative agreement is quite good with the exception of a phase shift at higher speeds for the UH–60A. The calculated amplitude of the bending moments is less than the measurements at all airspeeds and azimuths.

The 3/rev components of the midspan bending moments are examined in more detail in Figures 6 and 7 which show the amplitude and phase of the 3/rev load as a function of advance ratio for both aircraft. In each case the calculations include three different wake models: a free wake where the vortex elements are allowed to distort freely, a prescribed or rigid wake, and a Coleman model for the inflow that assumes

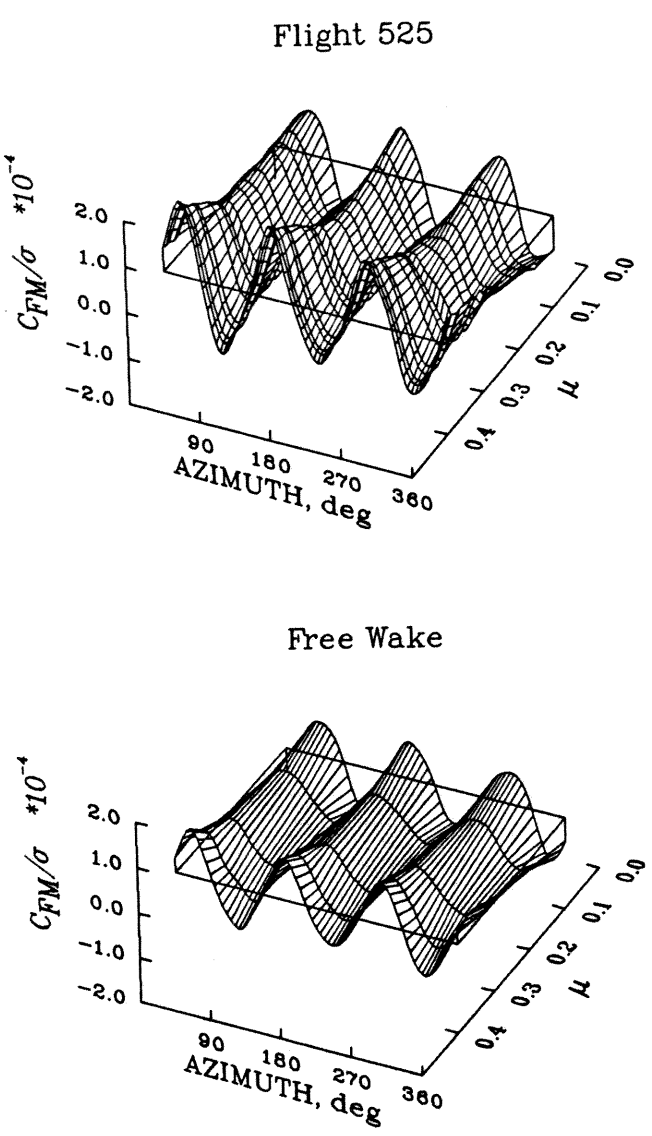

Figure 4. – Comparison of vibratory flap bending moments for the research Puma as a function of azimuth and advance ratio; 3–12 harmonics, $r/R = 0.57$.

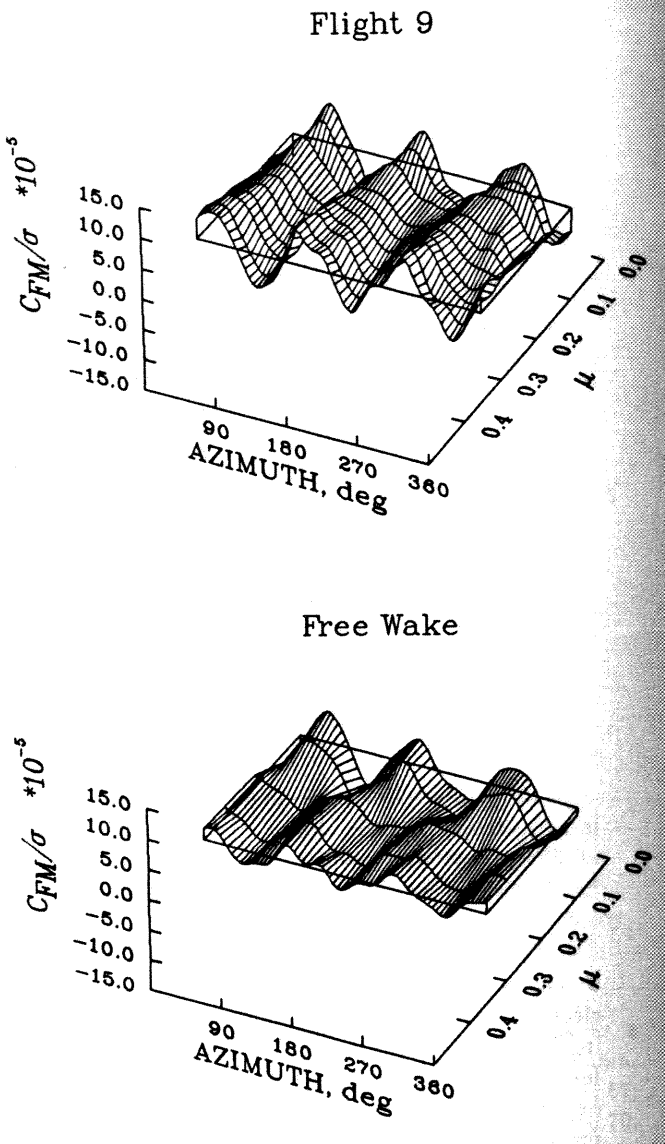

Figure 5. – Comparison of vibratory flap bending moments for the UH–60A Black Hawk as a function of azimuth and advance ratio; 3–12 harmonics, $r/R = 0.50$.

a uniform component plus a first harmonic cosine component. In the case of the Puma the prescribed and free wake models show excellent phase agreement with the midspan measurements and this is the basis for the good qualitative agreement noted in Figure 4. The Coleman wake model, on the other hand, leads the measured azimuth by about 60° for this harmonic. The phase angle of the third harmonic moment is simply $\tan^{-1}(b_3/a_3)$ where a_3 is the third harmonic cosine coefficient and b_3 is the third harmonic sine coefficient. In the azimuth reference of the rotor, however, this phase angle must be divided by the harmonic value so the 60° phase lead for the 3/rev loading is a 20° azimuth lead in the rotor reference. The free wake model provides the best prediction of the flap moment amplitudes for the Puma, showing the effects of the proximity of the tip vortices at low speed, the reduction in the vibratory load in the advance ratio range 0.2 to 0.3, and then the subsequent buildup in the vibratory load as advance ratio is increased. The amplitude of the 3/rev component, however, is underpredicted at all airspeeds.

The comparison of the calculations and measurements for the UH–60A, as shown in Figure 7, are not

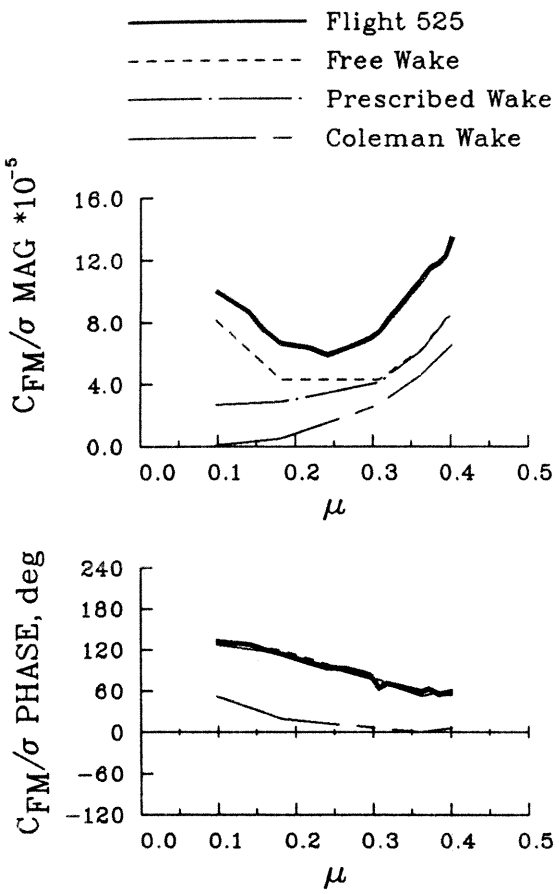

Figure 6. – 3/rev flap bending moments as a function of advance ratio for the research Puma; $r/R = 0.57$.

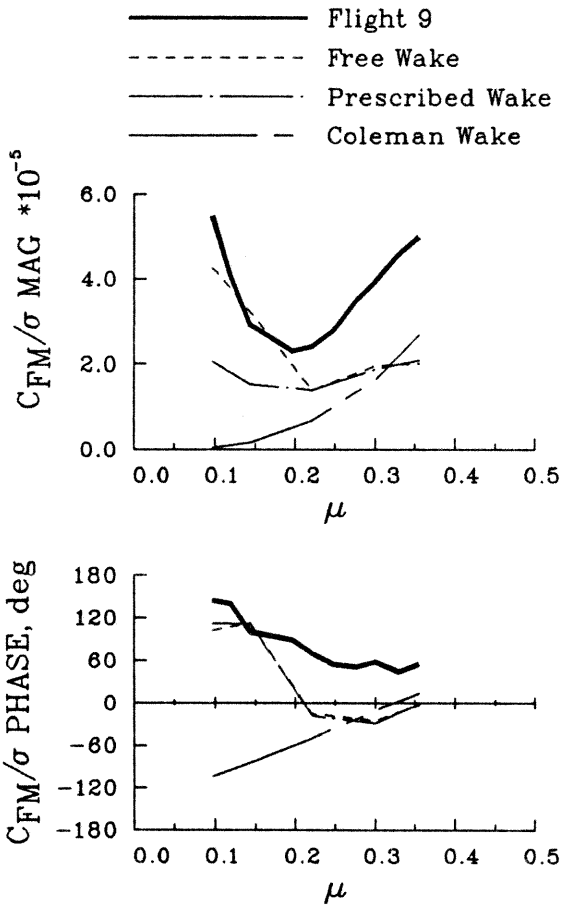

Figure 7. – 3/rev flap bending moments as a function of advance ratio for the UH–60A Black Hawk; $r/R = 0.50$.

as good as for the Puma. Specifically, at the higher speed conditions the midspan moments lead the measurements by 60° (20° in rotor azimuth) and this qualitative difference is noticeable in Figure 5 as well. As in the case of the Puma the free wake model provides the best prediction of the 3/rev amplitudes, but the loading is underpredicted at nearly all advance ratios.

The 4/rev flap bending moments moments are shown in Figures 8 and 9 at $0.67R$ for the Puma and $0.70R$ for the UH–60A. This outboard station is more suitable for comparison of the 4/rev loads as they are quite low at midspan. The 4/rev bending moments are roughly five times smaller than the 3/rev moments so their effect is not apparent in the surface plots of Figures 4 and 5. The Puma shows good qualitative agreement for this harmonic, but the predicted amplitudes are smaller than the measurements. The UH–60A calculations do not show good qualitative agreement with the data, especially at medium speeds where the calculations lag the measurements by about 120° (30° in rotor azimuth). However, the amplitude of the 4/rev flap bending moment at this station is fairly good for most advance ratios.

The physics of the vibratory flapping at low and high speed have features in common and ones that are different. In particular, at low speed the free wake calculation is clearly important, while at high speed the details of the wake model appear substantially less important. It is useful, therefore, to treat the two regimes separately to better focus on the problems involved in accurate prediction.

Low-Speed Vibratory Loads

Figures 10 and 11 compare the measured vibratory flap loads for the Puma and the UH–60A as functions of blade azimuth and radial station with the CAMRAD/JA free wake calculations. The 3/rev character of the data is evident and it appears that the

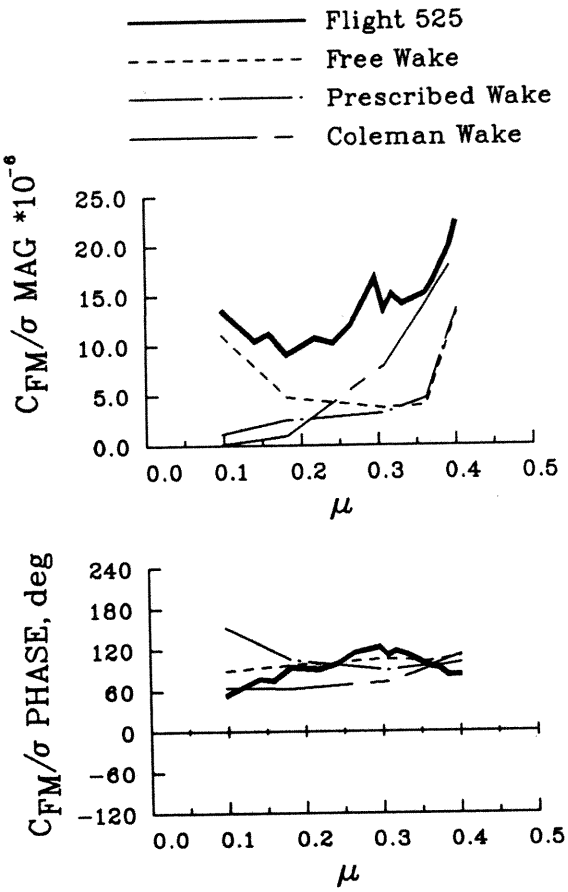

Figure 8. – 4/rev flap bending moments as a function of advance ratio for the research Puma; $r/R = 0.67$.

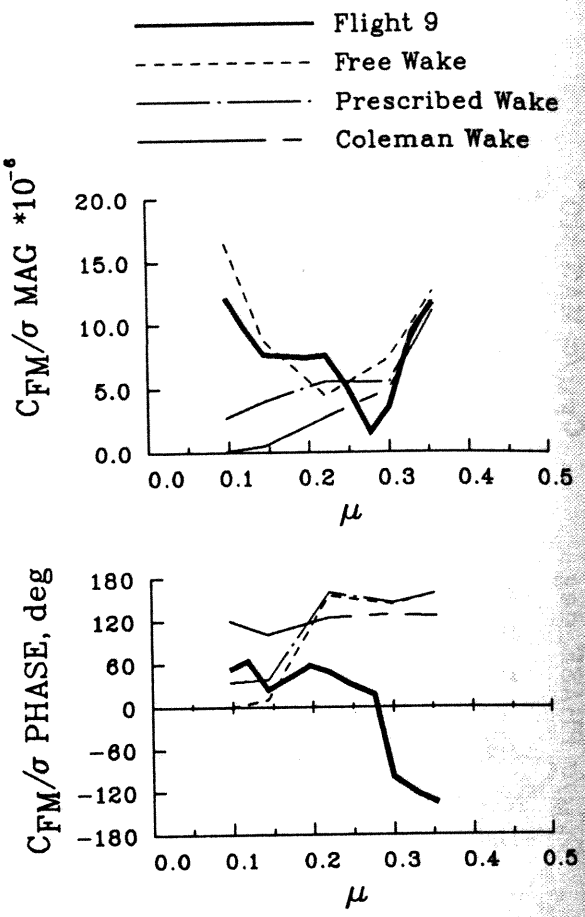

Figure 9. – 4/rev flap bending moments as a function of advance ratio for the UH–60A Black Hawk; $r/R = 0.70$.

midspan station provides a good representation of this behavior. As the blade second flap mode is approximately at 2.8/rev it is not surprising that the elastic deformation is primarily in this mode nor is it surprising that blade bending follows the moment mode shape of this mode. The radial moment distribution is less clearly defined for the UH–60A where measurements were obtained at only four stations. Unlike the Puma, the UH–60A calculations indicate that the loading is not so dependent on the second flap mode. Both rotors show the influence of higher frequency modes near the blade root.

Azimuthal plots are shown for the Puma and the UH–60A in Figures 12 and 13 for the midspan stations and in Figures 14 and 15 for the root or blade shank stations. The calculations include the free and prescribed wake models. The Coleman wake prediction is not included on these figures as the predicted moments are approximately zero at this airspeed. It is apparent from these figures that the free wake model provides a better prediction of the loads at this airspeed as is expected. The predicted phase for the research Puma is the same as measured, but the predicted phase for the UH–60A leads the measurements as was noted previously in Figure 7. The predicted flap bending moments show better agreement at the midspan station where the loading is dominated by the second flap mode. The root section predictions show the effects of the higher elastic modes and are not well predicted using the CAMRAD/JA model. This is especially true for the UH–60A prediction where the $0.113R$ measurement is made on the transition structure from the doublers to the blade clevis. This transition structure is an area of rapid change in mass and stiffness properties and causes difficulties with the CAMRAD/JA calculation[8] which uses the modal summation method to determine the bending moments.

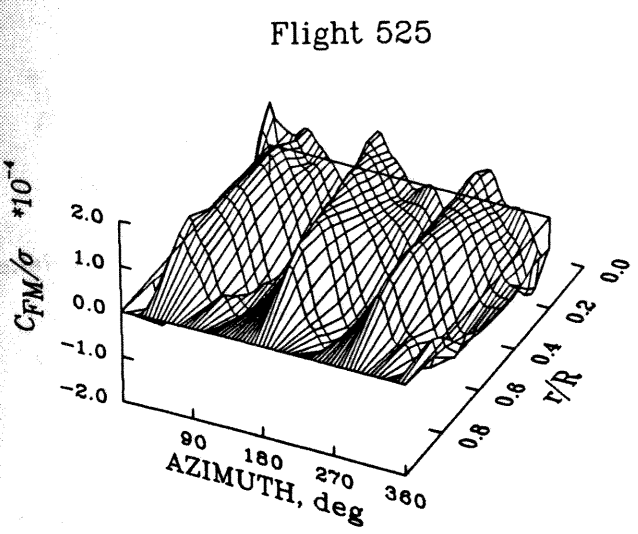

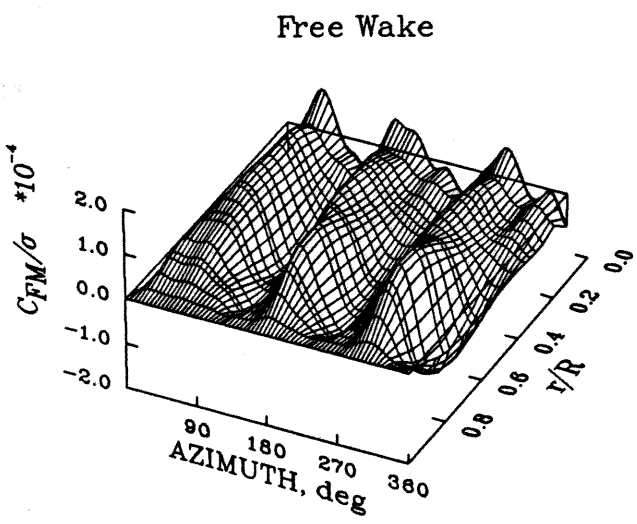

Figure 10. – Comparison of vibratory flap bending moments for the research Puma as a function of azimuth and radial station; 3–12 harmonics, $\mu = 0.098$.

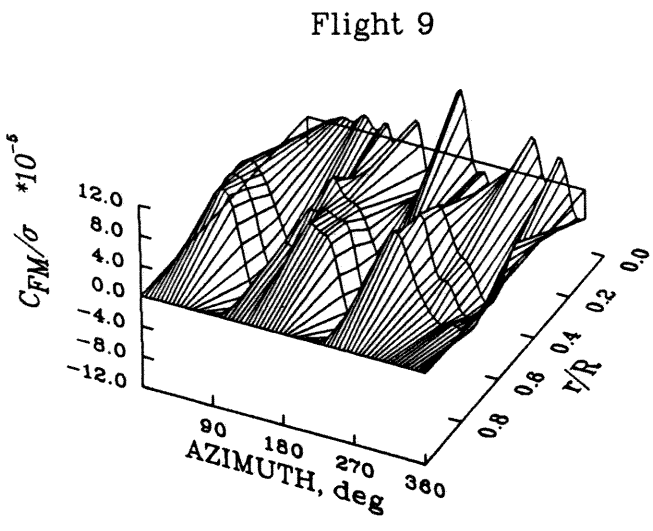

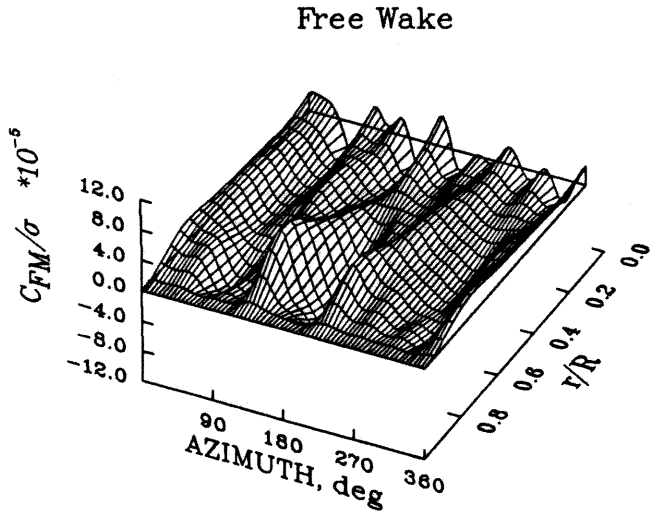

Figure 11. – Comparison of vibratory flap bending moments for the UH–60A Black Hawk as a function of azimuth and radial station; 3–12 harmonics, $\mu = 0.097$.

In examining the correlation shown in these figures it is useful to borrow some techniques from statistics, modify them slightly, and apply them to the problem as a means of characterizing how good or accurate the correlation is. This approach is useful as long as it is recognized that these measures must be interpreted carefully when applied to the deterministic problem that is being examined here. An example of this approach is shown in Figure 16 using the bending moment comparison from Figure 12. The azimuthal or time series signal of Figure 12 is transformed into cosine and sine harmonics $(a_0, a_1, b_1, \ldots)$ and the first five harmonic coefficients of the calculation are plotted as a function of the measurement harmonics. The calculated harmonic coefficients will lie on a 45° line if the agreement is exact. To the extent that the calculated harmonics are inaccurate they will be displaced from the 45° diagonal. The correlation is assessed by fitting a least squares regression line to the harmonics and comparing the slope, m, of the fit to unity, the slope of the diagonal. A second measure that is used is the correlation coefficient, r, and this provides a measure of dispersion of the calculation. The choice of the number of harmonics to be used in

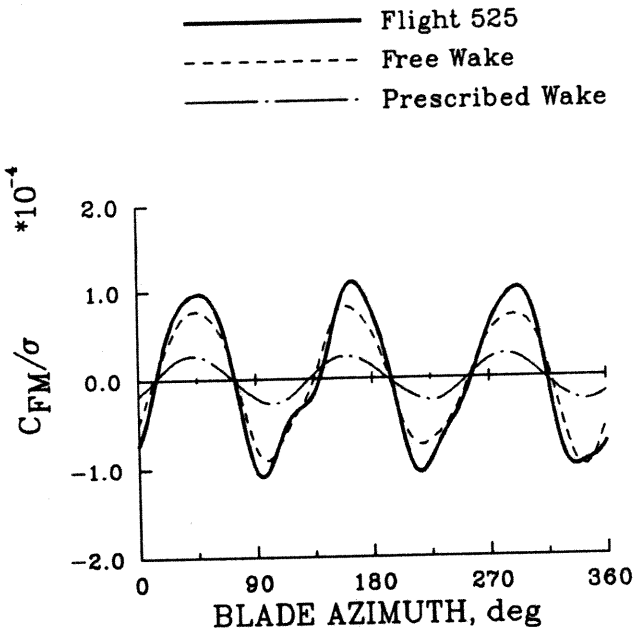

Figure 12. – Low-speed vibratory flap bending moment predictions for the research Puma; 3–12 harmonics, $r/R = 0.57$, $\mu = 0.098$.

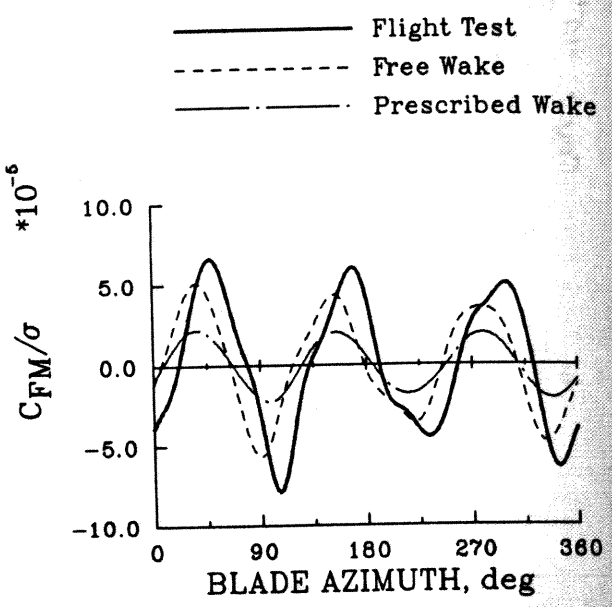

Figure 13. – Low-speed vibratory flap bending moment predictions for the UH–60A Black Hawk; 3–12 harmonics, $r/R = 0.50$, $\mu = 0.097$.

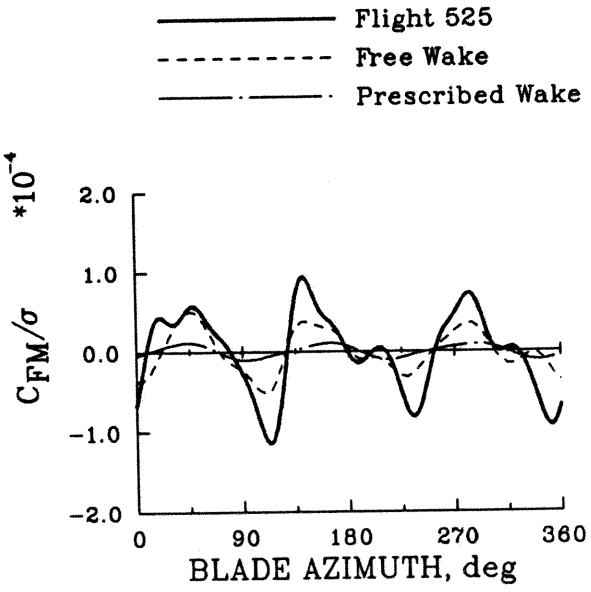

Figure 14. – Low-speed vibratory flap bending moment predictions for the research Puma; 3–12 harmonics, $r/R = 0.20$, $\mu = 0.098$.

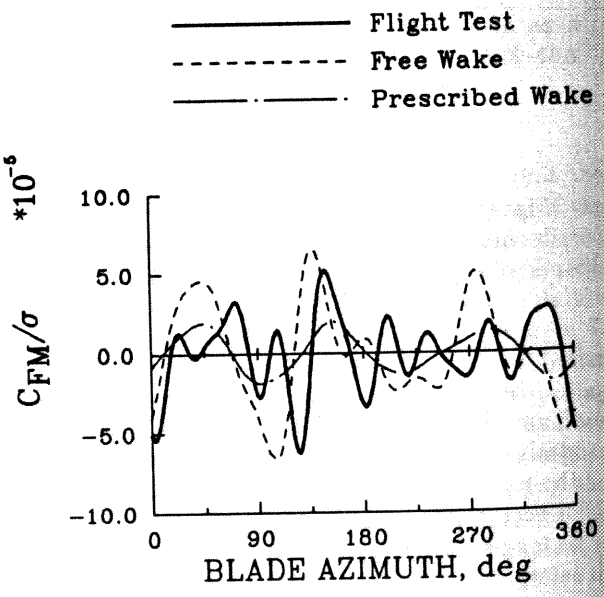

Figure 15. – Low-speed vibratory flap bending moment predictions for the UH–60A Black Hawk; 3–12 harmonics, $r/R = 0.113$, $\mu = 0.097$.

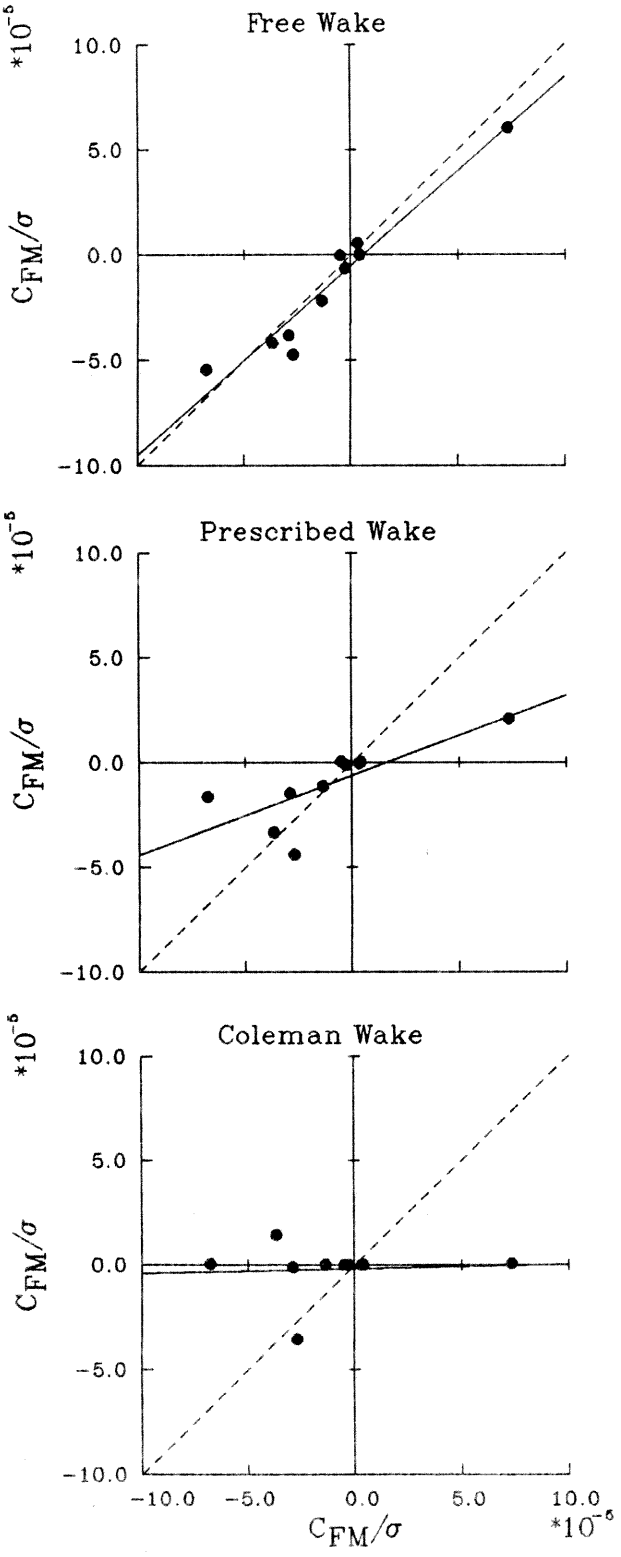

Figure 16. – Harmonic correlation for oscillatory flap bending moments for the research Puma; 1–5 harmonics, $r/R = 0.57$, $\mu = 0.098$.

the process affects the slope and correlation coefficient values to a degree, but not the relative rankings. This quantitative approach to correlation has the advantage that it tends to give more importance to the larger harmonics and their phase, which is similar to the the subjective approach taken by many analysts in judging the goodness of correlation. At the same time it is immediately evident which harmonics are poorly predicted, even when they are not the largest ones. This harmonic correlation process provides a convenient shorthand to use in comparing calculations and data and, in some cases, reduces the potential for self-delusion.

Referring to the harmonic correlation plots shown in Figure 16 it is seen that for the free wake the correlation is quite good. The slope in this case, 0.90, is about 10% low and the correlation coefficient is 0.97 which indicates that the dispersion is slight. The prescribed wake calculation is not as good as the free wake. The slope is 0.38 which is well below one and the correlation coefficient is 0.75 which indicates considerable dispersion. The Coleman wake calculation is essentially uncorrelated. The slope in this case is 0.02 and the correlation coefficient is 0.06.

The m and r values for the three wake models and the aircraft are tabulated in Table 1. The tabulated values show that the free wake model provides the best correlation but, in general, the amplitude is too low. The predictions are more accurate at the midspan, perhaps because of the importance of the second flap mode at this location. Inboard the correlation is not as good and the loading is more strongly influenced by the other modes. The correlation of the CAMRAD/JA free wake model with the UH–60A is not as good as for the research Puma and this is primarily a result of the approximately 15° phase lead that is seen in Figure 13 for the UH–60A. If the phase of the 3/rev loads is ignored and only the amplitude is examined then the predicted load is approximately 20 to 25% low for both aircraft.

Model Parameter Effects

The comparison of the CAMRAD/JA predictions of the flap bending moment with flight test data demonstrate that the wake model has a significant effect on the accuracy of the correlation. The effects of other model parameters is examined here by making changes in these parameters and comparing the results to the free wake calculation which is used as a baseline. In the case of the Puma, section lift measurements are available at $0.92R$, $0.95R$, and $0.978R$ and these data are particularly useful in assessing the effects of the model changes. Eleven changes from the baseline are

Table 1. – Slope and correlation coefficient values for flap bending moments at low speed; 1-5 harmonics.

	Midspan		Root	
	m	r	m	r
Puma:				
Free Wake	0.90	0.97	0.53	0.95
Prescribed Wake	0.38	0.75	0.16	0.77
Coleman Wake	0.02	0.06	0.01	0.05
UH–60A:				
Free Wake	0.70	0.75	0.42	0.20
Prescribed Wake	0.45	0.64	0.14	0.12
Coleman Wake	0.20	0.32	-0.10	-0.11

examined including the prescribed and Coleman wake models already discussed. The harmonic correlation m and r values are referred in each case to the flight measurements. These m and r values for the Puma are shown in Table 2 for the section lift at $0.95R$ and the flap bending moment at $0.57R$. Harmonic correlation values for the UH–60A are given in Table 3 for the flap bending moment at $0.50R$. Selected examples for the research Puma are shown in Figure 17 for the section lift at $0.95R$ and in Figure 18 for the flap bending moments at $0.57R$. Calculations for the UH–60A flap bending are shown in Figure 19.

Table 2. – Slope and correlation coefficient values for research Puma at low speed; 1-5 harmonics.

	$L(0.95R)$		$M_F(0.57R)$	
	m	r	m	r
Free wake (baseline)	1.42	0.91	0.90	0.97
Prescribed wake	0.83	0.84	0.38	0.75
Coleman wake	0.22	0.34	0.02	0.06
Increased core size	1.32	0.94	0.78	0.95
Decreased core size	1.63	0.87	1.11	0.98
Linear aero	1.36	0.91	0.87	0.97
Straight blade	1.39	0.93	0.97	0.96
No yawed flow	1.41	0.92	0.90	0.97
Add'l bending/torsion	1.41	0.91	0.86	0.97
No bending modes	1.45	0.92	–	–
No torsion modes	1.32	0.92	0.81	0.95
No unsteady aero	1.35	0.92	0.85	0.95

The CAMRAD/JA lift on the Puma at $0.95R$ is overpredicted as seen in Figure 17 and also as indicated by the harmonic coefficient slope of 1.42 in Table 2. There is good qualitative agreement, as shown in Figure 17, and this is also indicated by the correlation coefficient of 0.91 in Table 2. The prescribed wake calculation, by comparison, is less accurate and the Coleman wake model is clearly inadequate.

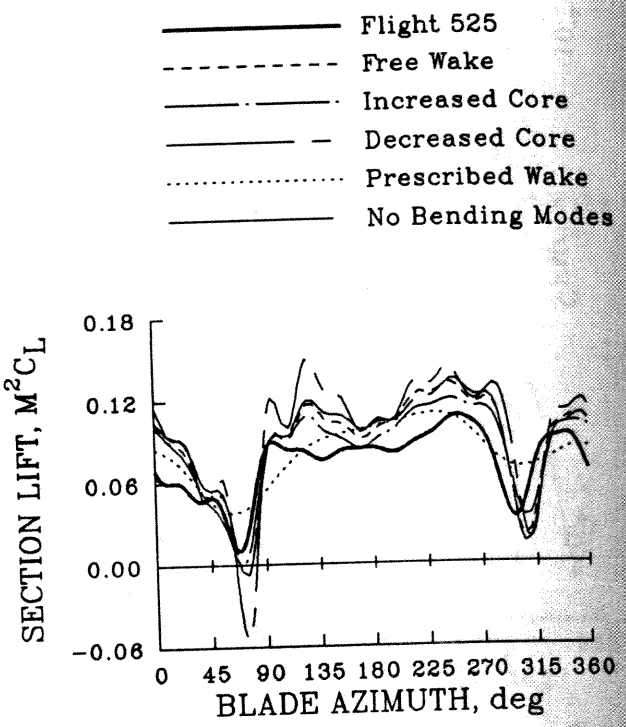

Figure 17. – Comparison of measured and calculated section lift for the research Puma with modeling changes; 0–12 harmonics, $r/R = 0.95$, $\mu = 0.098$.

Table 3. – Slope and correlation coefficient values for UH–60A at low speed; 1-5 harmonics.

	$M_F(0.50R)$	
	m	r
Free wake (baseline)	0.70	0.75
Prescribed wake	0.45	0.64
Coleman wake	0.20	-0.10
Increased core size	0.66	0.75
Decreased core size	0.75	0.73
Linear aero	0.73	0.77
Straight blade	0.80	0.77
No yawed flow	0.71	0.75
Add'l bending/torsion	0.72	0.77
No torsion modes	0.75	0.77
No unsteady aero	0.74	0.74

The tip vortex core size was varied in CAMRAD/JA to examine its effects on the calculation. The baseline value of $0.035R$ (or $0.49c$) was increased to $0.055R$ and decreased to $0.015R$. An increase in the core size reduces the peak velocities in the vortex wake and reduces the loads on the blade. The airload decreases approximately 7% for the Puma and the bending moments decrease about 13% for the Puma and

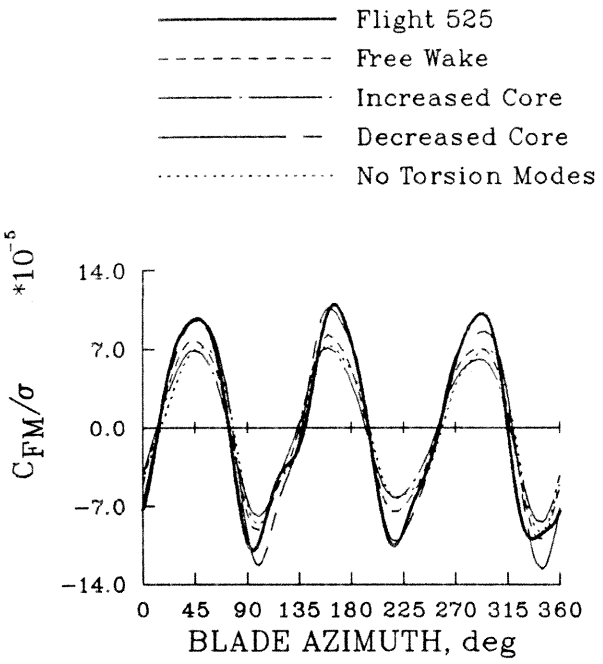

Figure 18. – Comparison of measured and calculated vibratory flap bending moments for the research Puma with modeling changes; 3–12 harmonics, $r/R = 0.57$, $\mu = 0.098$.

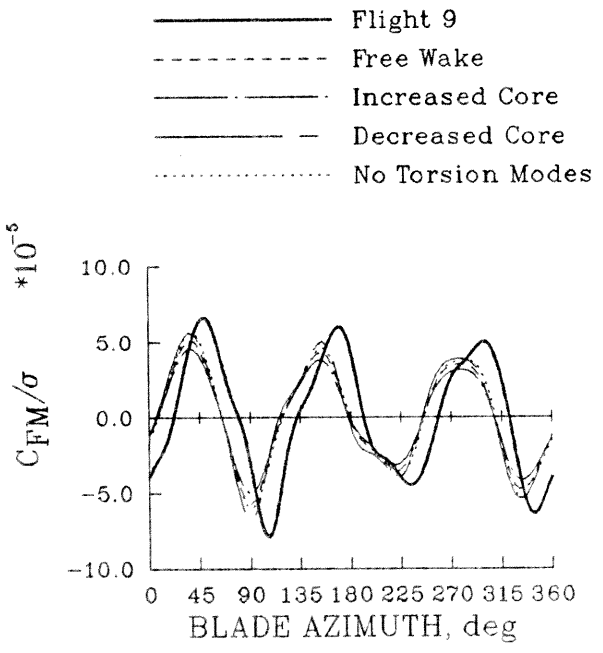

Figure 19. – Comparison of measured vibratory flap bending moments for the UH–60A Black Hawk with modeling changes; 3–12 harmonics, $r/R = 0.50$, $\mu = 0.097$.

6% for the UH–60A as shown in Tables 2 and 3 and in Figures 17 to 19. A decrease in the core size radius causes an increase in the blade loads and this increase is quite sizeable for the Puma at 23% but the UH–60A bending moments increase only 7%.

The effects of the Puma and UH–60A airfoils was assessed by replacing the two-dimensional lift, drag and moment data in CAMARD/JA with synthesized data for a hypothetical airfoil with a constant lift curve slope, constant drag, and constant pitching moment. However, the static stall model used in all the CAMRAD/JA calculations was retained. This linear aerodynamic model shows a slight reduction in the loads for the Puma and a small increase in the loading for the UH–60A.

Sweep effects were investigated by setting the aerodynamic center offsets to zero and eliminating sweep corrections in using the two-dimensional airfoil tables. Setting these aerodynamic offsets to zero effectively defines an aerodynamically straight blade. This change shows a slight decrease in the airload at the tip of the Puma blade, but an increase in the bending moments for both the Puma and the UH–60A.

The section lift, drag, and moment coefficients are modified in CAMRAD/JA depending upon yawed flow. The effect of removing the yawed flow corrections was examined and, as shown in Tables 2 and 3, this had very little effect upon the calculated loads.

The CAMRAD/JA baseline model uses six bending modes to represent the bending degrees of freedom for the two aircraft. The model uses two torsion modes for the Puma and three torsion modes for the UH–60A. The effect of using additional modes was investigated by increasing the number of bending modes to ten and the number of torsion modes to five, but no effect is observed in Tables 2 and 3. The effect of reducing the number of blade bending degrees of freedom was looked at by removing four bending modes and modeling the blade as a rigid, articulated blade. For this case the baseline torsion modes were retained. The effect of this change was slight as shown in Figure 17 and in Table 2. The airloads for this low-speed condition were not influenced by the blade elastic motion in bending. In a complementary manner, the bending modes were retained and the torsion modes removed and this shows about a 10% reduction in the airload as shown in Table 2. This reduction is also seen in the Puma midspan bending moments, but not in the UH–60A where there is a slight increase in the bending moments as shown in Figure 19.

Finally, the effect of unsteady aerodynamics was examined by eliminating the unsteady terms from the aerodynamic calculation. Attempts to calculate

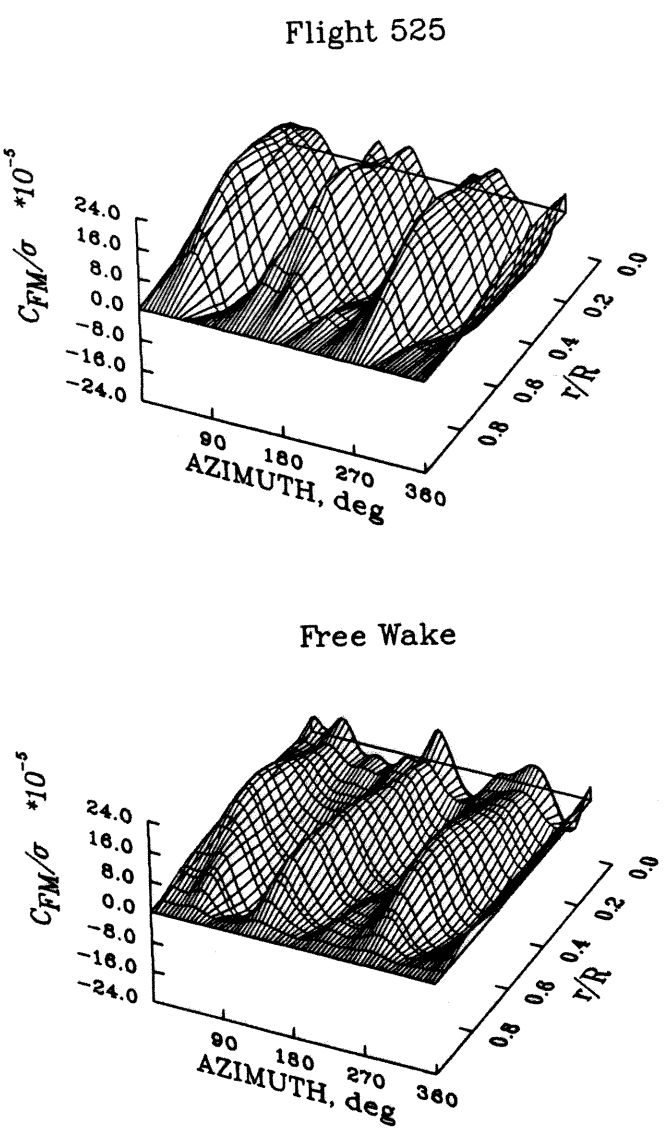

Figure 20. – Comparison of vibratory flap bending moments for the research Puma as a function of azimuth and radial station; 3–12 harmonics, $\mu = 0.402$.

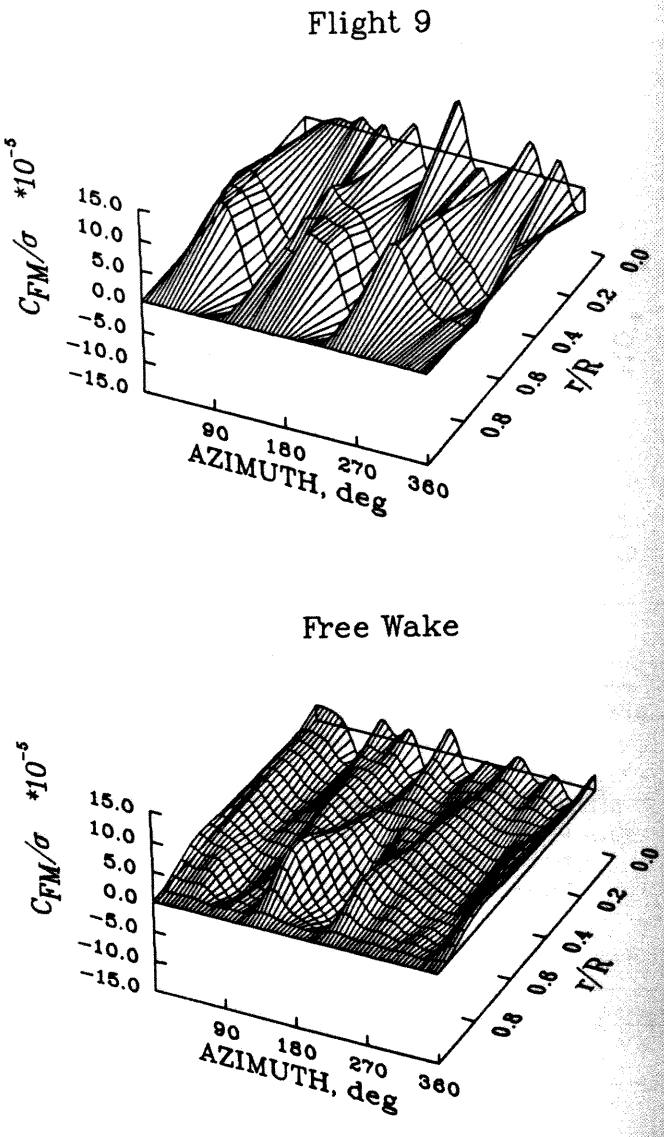

Figure 21. – Comparison of vibratory flap bending moments for the UH–60A Black Hawk as a function of azimuth and radial station; 3–12 harmonics, $\mu = 0.355$.

this effect for the baseline case were unsuccessful because of convergence problems so the removal of the unsteady aerodynamics was restricted to the case without torsion degrees of freedom. Thus, the change for this case needs to be compared to the case without torsion degrees of freedom rather than the baseline. The effects of unsteady aerodynamics in this low-speed case were slight.

Most of the model parameter changes examined here have little effect on the predicted flap vibratory loads for the Puma or the UH–60A. The one exception is the free wake model and this has a major impact on the loads that are predicted. Details of the free wake model, such as the assumed core size also influence the loads, but these effects are smaller. Changes in the blade dynamic models have very little influence on the calculated loads.

High-Speed Vibratory Loads

The measured and calculated flap bending moments are shown as functions of azimuth and radial station in Figures 20 and 21 for the Puma and the UH–60A. The azimuthal and radial distribution of the moments is similar to the distribution at low speed and, again, this loading is dominated by the second

flap mode. Near the blade root the effects of higher blade modes are noticeable.

The measured and calculated flap bending moments are compared for the two aircraft at midspan in Figures 22 and 23 and at the root location in Figures 24 and 25. The harmonic coefficient correlation parameters are tabulated in Table 4. Good phase agreement is seen for the Puma at midspan when comparing the free and prescribed wake predictions with data, but the amplitude is underpredicted. Unlike the low-speed case, the moments predicted by CAMRAD/JA are essentially identical for the two wake models at this speed. The Coleman wake model shows a similar moment amplitude but the predicted phase leads the data. In the case of the UH–60A the amplitude of the midspan bending moment is also underpredicted and each of the wake models show a phase lead with respect to the data. The predicted flap bending moments at the blade root show poor agreement with the measurements and this is especially true for the UH–60A inboard station.

Table 4. – Slope and correlation coefficient values for flap bending moments at high speed; 1-5 harmonics.

	Midspan		Root	
	m	r	m	r
Puma:				
Free Wake	0.75	0.92	0.44	0.75
Prescribed Wake	0.74	0.92	0.43	0.74
Coleman Wake	0.65	0.70	0.34	0.51
UH–60A:				
Free Wake	0.60	0.79	-0.24	-0.37
Prescribed Wake	0.61	0.79	-0.25	-0.39
Coleman Wake	0.85	0.78	-0.32	-0.35

Model Parameter Effects

The comparison of the CAMRAD/JA predictions with flight test measurements using the three wake models suggests that the wake modeling is less important at high speed than at low speed. It is useful to examine the effects of other model parameters just as was done in the low-speed case. The previous model parameter examination is repeated here except that the prescribed wake model is used as the baseline case instead of the free wake model and vortex core size variation is not considered. As before, section lift data at $0.95R$ from the research Puma are used to gain insight into the aerodynamic loading environment as various model parameters are changed. The harmonic coefficient correlation parameters for the various cases are shown in Table 5 for the Puma and in Table 6 for the UH–60A. Each calculation is referred to the flight test measurements and the m and r values are to be compared with the prescribed wake baseline to determine modeling or parameter effects. Selected cases for the Puma section lift are shown in Figures 26 and 27 and for the flap bending moments in Figure 28. Flap bending moment cases for the UH–60A are shown in Figure 29.

Table 5. – Slope and correlation coefficient values for research Puma at high speed; 1-5 harmonics.

	$L(0.95R)$		$M_F(0.57R)$	
	m	r	m	r
Prescribed wake	1.01	0.95	0.74	0.92
Coleman wake	2.30	0.98	0.65	0.70
Linear aero	0.83	0.70	0.73	0.78
Straight blade	0.92	0.94	0.78	0.93
No yawed flow	1.00	0.96	0.71	0.92
Add'l bending/torsion	1.03	0.95	0.74	0.93
No bending modes	1.02	0.95	–	–
No torsion modes	0.97	0.94	0.70	0.89
No unsteady aero	0.97	0.95	0.68	0.88

Table 6. – Slope and correlation coefficient values for UH–60A at high speed; 1-5 harmonics.

	$M_F(0.50R)$	
	m	r
Prescribed wake	0.61	0.79
Coleman wake	0.75	0.78
Linear aero	0.55	0.83
Straight blade	0.57	0.71
No yawed flow	0.61	0.79
Add'l bending/torsion	0.59	0.80
No torsion modes	0.55	0.81
No unsteady aero	0.52	0.78

The section lift predicted by CAMRAD/JA using the prescribed wake shows very good agreement with the measured data (Figure 26). Although the lift calculated at this outboard station is within 1% of the measurements the flap bending moments are about 25% low. A similar disparity was noted at low speed, although in that case the lift at $0.95R$ was overpredicted while the flap bending moments were underpredicted by about 10%. The Coleman wake model calculation shows behavior similar to the prescribed wake, but the amplitude is excessive. Qualitatively, this wake model is correctly modeling the effect of aircraft trim as speed is increased although it does not model the vortex wake at low speeds.

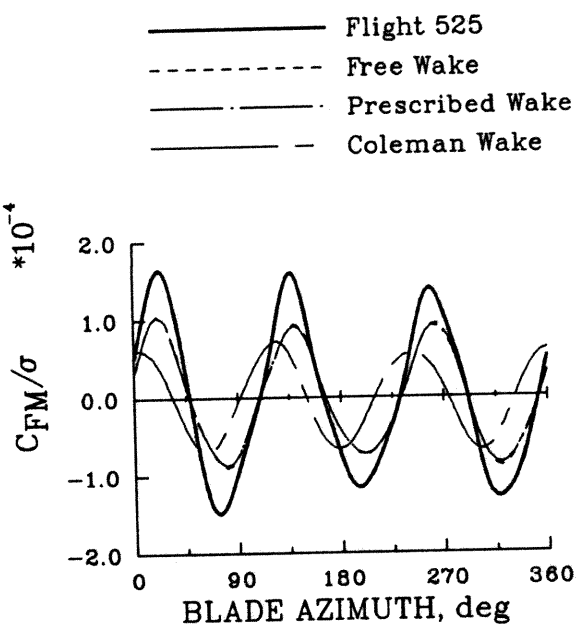

Figure 22. – High-speed vibratory flap bending moment predictions for the research Puma; 3–12 harmonics, $r/R = 0.57$, $\mu = 0.402$.

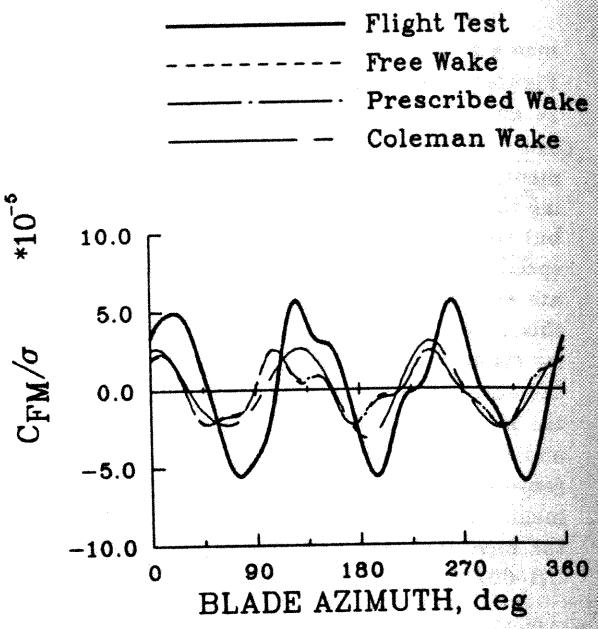

Figure 23. – High-speed vibratory flap bending moment predictions for the UH–60A Black Hawk; 3–12 harmonics, $r/R = 0.50$, $\mu = 0.355$.

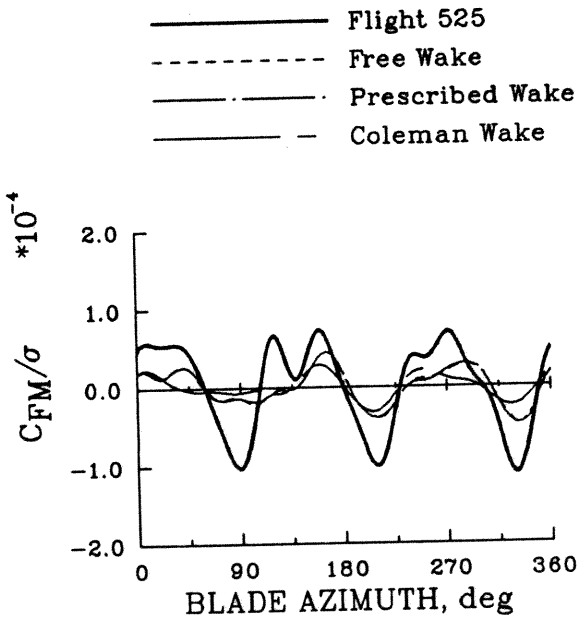

Figure 24. – High-speed vibratory flap bending moment predictions for the research Puma; 3–12 harmonics, $r/R = 0.20$, $\mu = 0.402$.

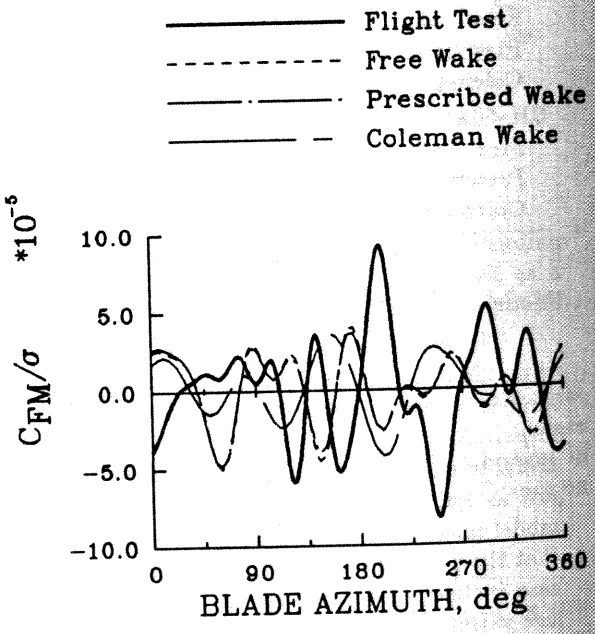

Figure 25. – High-speed vibratory flap bending moment predictions for the UH–60A Black Hawk; 3–12 harmonics, $r/R = 0.113$, $\mu = 0.355$.

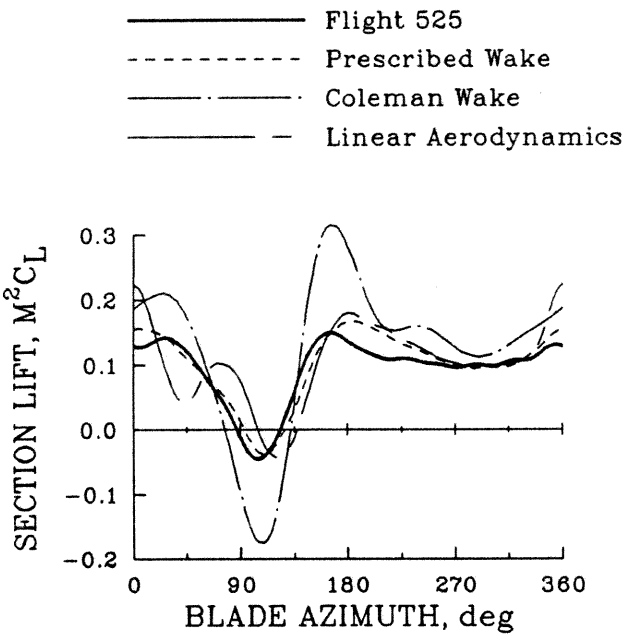

Figure 26. – Comparison of measured and calculated section lift for the research Puma with aerodynamic modeling changes; 0–12 harmonics, $r/R = 0.95$, $\mu = 0.402$.

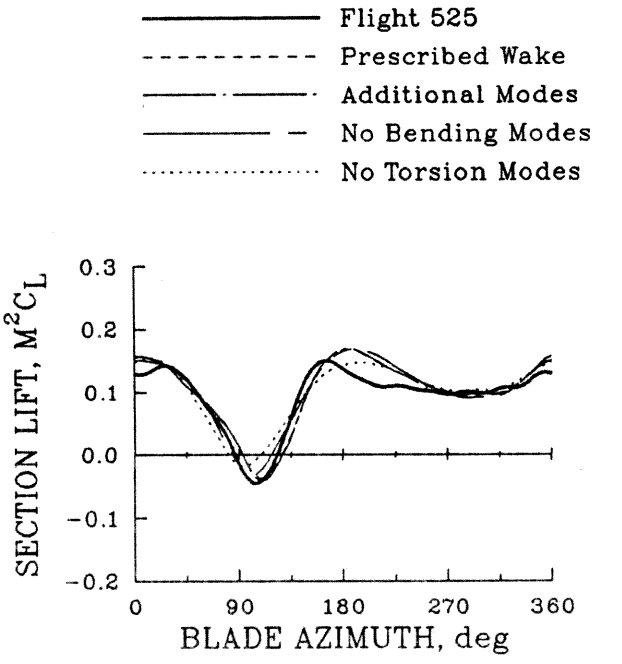

Figure 27. – Comparison of measured and calculated section lift for the research Puma with structural modeling changes; 0–12 harmonics, $r/R = 0.95$, $\mu = 0.402$.

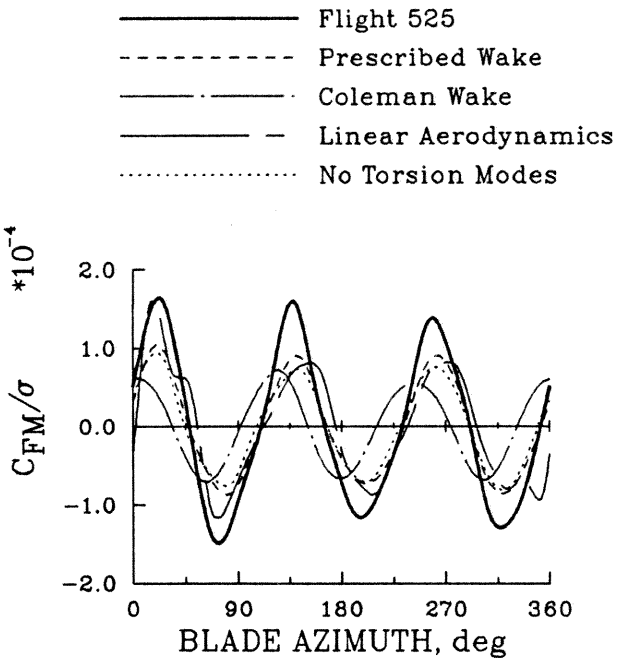

Figure 28. – Comparison of measured and calculated vibratory flap bending moments for the research Puma with modeling changes; 3–12 harmonics, $r/R = 0.57$, $\mu = 0.402$.

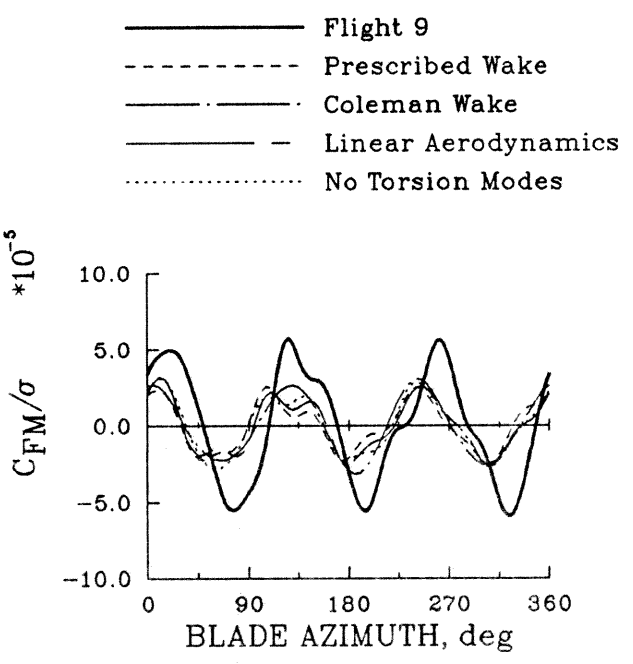

Figure 29. – Comparison of measured and calculated vibratory flap bending moments for the UH–60A Black Hawk with modeling changes; 3–12 harmonics, $r/R = 0.50$, $\mu = 0.097$.

The effect of using the linear aerodynamic model instead of the airfoil tables is significant for this high-speed case. The blade elastic motion for frequencies greater than 3/rev is substantially increased. The predicted lift is altered on the advancing side of the disk as shown in Figure 26 and the resulting flap bending moments are also changed, but the mechanism is not clear.

Changing the blade aerodynamic center offsets to zero reduces the lift at the blade tip by about 10% for the Puma. The bending moment at midspan increases slightly for the Puma while there is a slight decrease for the UH–60A. Less effect is observed when the yawed flow corrections are removed.

Increasing the number of bending and torsion modes has no significant effect on the resulting airloads or bending moments. Noticeable effects are seen, however, if the bending or torsion degrees of freedom are removed, as shown in Figure 27. In the latter case the amplitude of the vibratory response is reduced about 5%. Little effect is seen in these calculations when the unsteady airloads are not included.

Most of the modeling parameters examined at high speed have only a small effect on the accuracy of the CAMRAD/JA predictions of the vibratory flap bending moments. The only exceptions are the Coleman wake and the use of linear aerodynamics and their poor performance is not surprising considering the level of approximation involved.

DISCUSSION

CAMRAD/JA meets the first test of analytical methods in the case of the research Puma in its ability to predict the qualitative nature of the flap vibratory loads over a wide range of airspeeds. This is evidenced by the good phase agreement that is seen for the 3/rev and 4/rev loads in Figures 6 and 8. This qualitative test is not met for the UH–60A and the reasons for this are unclear. The calculated flap loads at 3/rev lead the measurements from 10 to 20° in rotor azimuth depending upon airspeed and slightly greater differences are seen for the 4/rev loads. As the measurements on the two rotor systems agree with each other quite well it seems likely that the poor qualitative agreement for the UH–60A is related to the CAMRAD/JA modeling of the aircraft. The section lift values calculated on both rotors near the blade tip at high speed show good agreement in phase as indicated in Figure 30. However, there is a different phase shift in the calculated response as is seen in comparing Figures 6 and 7 for the 3/rev component. Structurally the two rotors are quite similar and the modal frequencies calculated in a vacuum compare

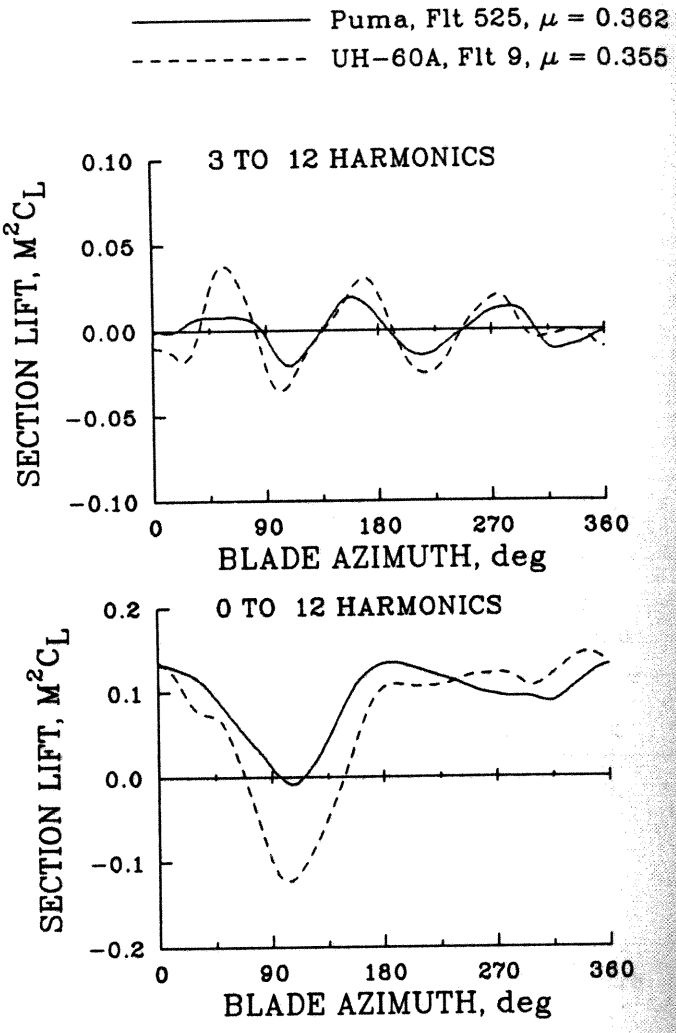

Figure 30. – Comparison of calculated Puma and UH–60A airloads at $r/R = 0.95$.

quite well for the lower modes as shown in Figure 31. The reasons for the different responses calculated here are not understood. It is expected that the detailed airload and structural measurements that will be obtained from the UH–60A in the future[6] will allow a direct determination of the blade response[7] to compare with the predicted response and this will provide a means of understanding the differences noted here. In addition it is anticipated that the extensive structural testing of the UH–60A blades that has been performed[8] will provide a more accurate structural model for use in future calculations.

The CAMRAD/JA predictions of the 3/rev and 4/rev amplitudes are generally lower than the measurements at all airspeeds, as shown in Figures 6 to 9. An exception is observed for the UH–60A 4/rev

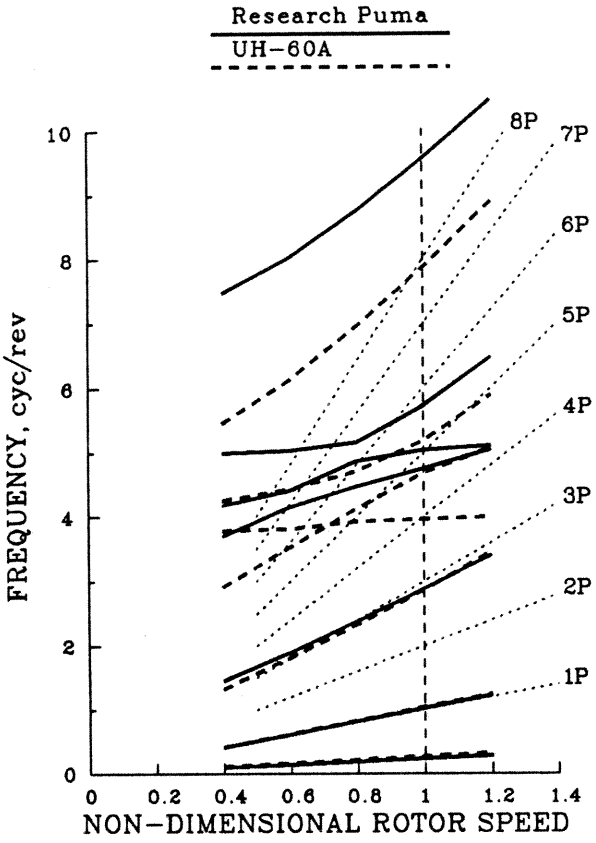

Figure Figure 31. – Calculated modal frequencies for Puma and UH–60A.

loads where the amplitude shows fair to good agreement with the measurements at most airspeeds, despite the differences in phase. The CAMRAD/JA calculated section lift at the tip of the research Puma is overpredicted at low speed but quite close to the measurements at high speed. The difference in the correlation for the lift and bending moments suggests that there may be substantial differences between predicted and actual airloads inboard on the Puma blade where no measurements are available. However, it is interesting to note that a different analysis, developed by the DRA and Westland Helicopters, has achieved substantially better results for this same case.[2] The availability of detailed airload and structural measurements on the UH–60A in the future will provide a more accurate test of the CAMRAD/JA analysis' ability to correctly predict the amplitude of the vibratory flap bending moments.

The comparison of the CAMRAD/JA predicted vibratory flap loads at low speed with the measurements clearly shows the importance of the wake model in the prediction of these loads. This importance has long been recognized and was a major incentive in the development of both the prescribed wake[9] and the free or distorting wake as discussed in Ref. 10. The variation in modeling parameters shown here suggests that the accuracy of the prediction is most strongly dependent upon the calculation of the vortex wake. Other aerodynamic effects and the blade dynamic model have little effect on the accuracy of the prediction. It is important to note, however, that although aeroelastic effects caused by blade bending or torsion are not important the effect of blade rigid flapping is important for the present calculation and must be included.

The Puma section lift measurements, shown in Figure 17, show that the loading is dominated by vortex-induced airloads on the advancing and retreating sides of the disk. It is possible from these data and pressure measurements obtained at $0.89R$, $0.92R$, and $0.978R$ to define the core diameter of an "apparent vortex" that induces the loads that are seen. The edges of the core are identified by the positive and negative peaks of pressure in the time histories and these peaks are plotted onto the rotor disk to identify the core location and size. Using this approach the core diameter of the apparent vortex is approximately $1.2c$ on the advancing side and $2.6c$ on the retreating side. However, in the CAMRAD/JA free wake model each core has a diameter of approximately $0.5c$. The difference in size between the core that is in the math model of the vortex wake and the apparent core that is inferred from the data is a result of both additive effects of multiple vortices in the wake and the distance of the probe (the blade pressure transducers) from the centroid of these vortices. The CAMRAD/JA calculations provide considerable insight into the geometry of the wake and the effects that are seen on the blade. Figure 32 shows the CAMRAD/JA predicted locations of the blade tip vortices for the prescribed wake and Figure 33 shows the locations for the free wake. The calculations in each figure are for a blade azimuth position of 75°, just when the blade is in the middle of the apparent vortex on the advancing side of the disk. Figures 32(b) and 33(b) show a disk-plane view of the tip vortices from the previous blades. Figures 32(a) and 33(a) show the intersection of these tip vortices with a vertical plane through the blade quarter chord. Note that the disk-plane view is limited to four tip vortices, but the intersection plane shows additional (older) vortices as well. The traces of the tip vortices for the prescribed wake follow a smooth trajectory as is expected. The older the vortex, the further it is from the blade. However, in the case of the free wake calculation the vortices are closely interacting with each other and

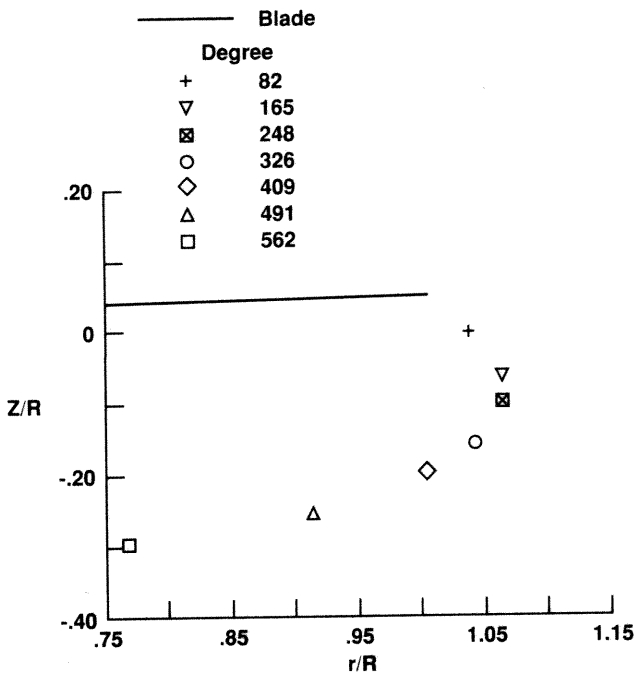

a. Blade plane view.

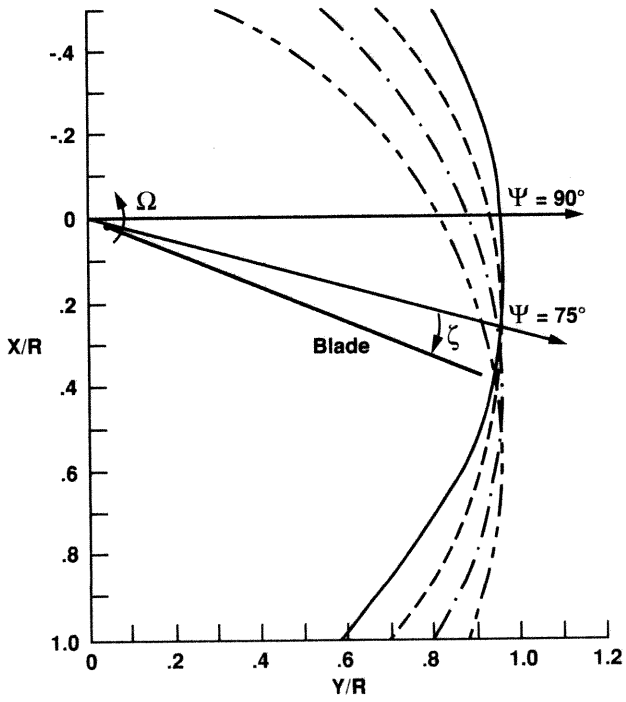

b. Disk plane view.

Figure 32. – Calculated prescribed wake tip vortex positions for the research Puma; $\psi = 75°$, $\mu = 0.098$.

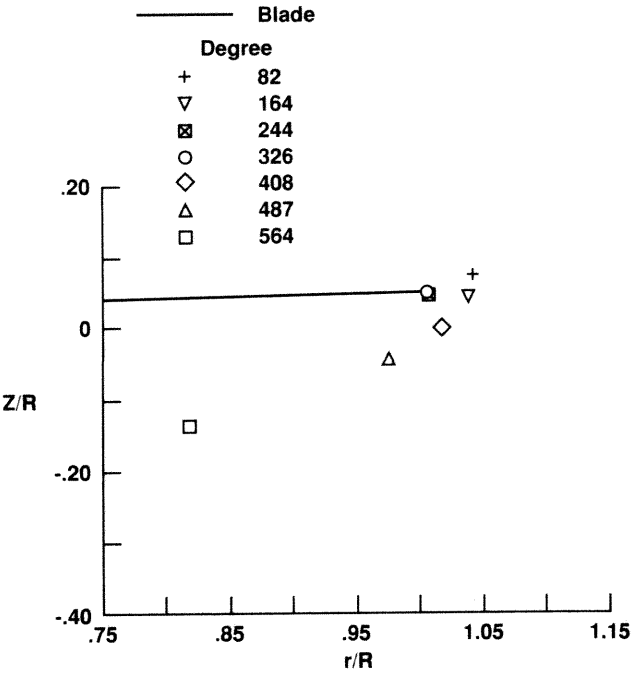

a. Blade plane view.

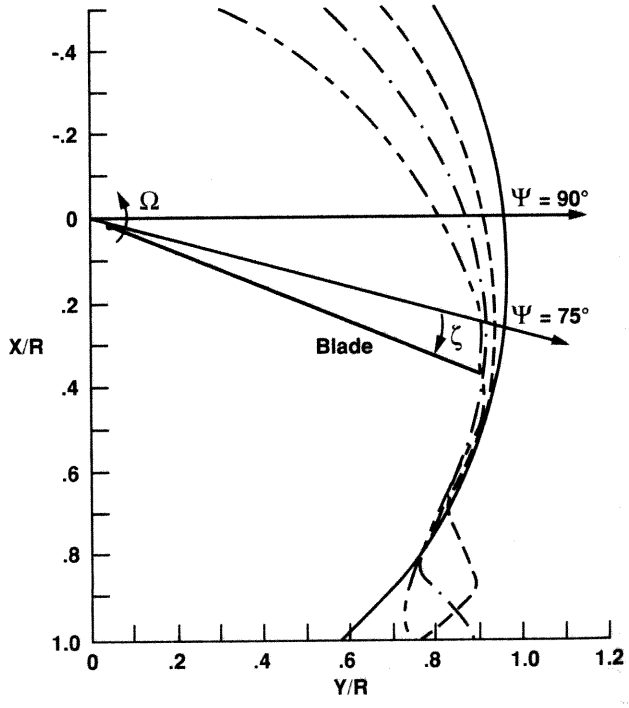

b. Disk plane view.

Figure 33. – Calculated free wake tip vortex positions for the research Puma; $\psi = 75°$, $\mu = 0.098$.

the blade. It is the additive effects of these vortices that causes the apparent vortex that is observed in the blade airload measurements. The 3/rev and 4/rev vibratory flap bending moments that are the source of vibration in the fuselage depend upon the amplitude of this apparent vortex and the duration between the positive and negative peaks. The CAMRAD/JA free wake model appears to provide a good physical representation of the vortex wake for the case shown here, although the data supporting this conclusion are somewhat indirect. The interaction of the blade and the tip vortices are clearly fundamental to an accurate prediction of the vibratory loading. Some aspects of this free wake model are empirical in nature, particularly having to do with the size of the tip vortex core, its growth, and how it interacts with the blade. Until better measurements are obtained to describe these behaviors it may not be possible to significantly improve these predictions.

The vibratory flapping loads at high speed, unlike the low-speed loads, are the same for the prescribed or free wake models. In part this is because the tip vortices are more spread out so that the relative distortion of the vortex geometry is less, but also because the tip vortices are convected away from the disk plane before the passage of the next blade. That a free wake model is not needed at high speed to predict the vibratory loads remains a controversial topic[11] and this may be in part because available wind tunnel data[12] have tended to focus airloads research on lift and shaft angle-of-attack conditions where the blade vortices are not convected away from the rotor disk. It is important to note, however, that under some flight conditions, such as autorotation, where the rotor disk comes in close proximity to the vortex wake it may be necessary to use a free wake analysis to provide a good calculation of the vibratory flap loads. Under normal, high-speed, level flight conditions, however, the effect of the distorted vortex wake is not important for vibratory flap load prediction.

The vibratory flapping loads at high speed are largely a consequence of the aircraft trim, that is, the need to maintain roll moment balance rather than a function of the rotor's vortex wake as at low speed. Figure 30 shows that the airloads at the blade tip are greatly reduced at the start of the second quadrant or even negative. The airload is reduced in this quadrant to keep the rolling moment near zero. The harmonic form of these airloads emphasizes odd harmonics to a degree and the loading decreases as harmonic number goes up. As shown in Figure 30 the vibratory loading is dominated by the 3/rev airloads and the phase of these loads corresponds directly to the reduced airload in the second quadrant that is forced by aircraft roll moment balance. Although the aeroelastic effects appear to be more important at these high-speed conditions than for the low-speed case, the influence on the vibratory flap airloads is still fairly small as noted in Figure 27, where the blade is modeled as a rigid, articulated blade.

At high speed, the simplest wake model, such as the Coleman wake, tends to overpredict the airloads, but gives the best prediction of the vibratory bending moments. This has been noted for other analyses and other data sets.[13,14] As modeling complexity and sophistication is added to the Coleman wake, as an example, the airloads at high speed tend to be reduced. This gives the appearance of a paradox, that is, as modeling sophistication increases the correlation becomes worse. It is not a paradox, however, but simply evidence that more work is required in the area of rotor vibratory loads before prediction can be used in design.

The flap bending moment correlation shown in this paper is significantly better for midspan stations where the second flap mode has the largest effect than for the root sections where the higher modes are also important. The CAMRAD/JA model obtains the moments at any radial station using modal summation. For a radial station where there are rapid stiffness changes, such as near the blade root for the Puma and the UH–60A, the moment calculation is inaccurate. It is anticipated that finite-element based analyses will be able to show more accurate predictions of the loads in areas of rapid stiffness change and it is important in future correlation efforts to demonstrate improvements in these areas. For the articulated rotors considered here it may be that an accurate prediction of blade root loads is unimportant from a vibration point of view, but for hingeless or bearingless rotors these predictions may be far more important than the midspan predictions.

CONCLUSIONS

The CAMRAD/JA analysis has been used to model two aircraft, the research Puma and the UH–60A, and the resulting predictions have been compared with flight test data. The comparison has examined the prediction of flap vibratory loads, the loads at 3/rev and higher, and the test for the analysis has been to demonstrate that it matches both the qualitative and quantitative aspects of the measured flight data. In addition, limited investigations of the effects of modeling changes in the analysis have been made to better understand the correlation. From this effort the following conclusions are made:

1. The 3/rev flap bending moments are underpredicted at all flight speeds for both aircraft. The 4/rev flap bending moments are underpredicted for the research Puma, but the predictions show good agreement with the UH–60A 4/rev loads. None of the modeling changes examined explain the underprediction noted here.
2. The qualitative nature of the flap vibratory loads are well predicted by the analysis at all flight speeds for the Puma, but there is a phase lead in the UH–60A predictions that degrades the correlation. The cause of the phase lead is not understood.
3. The vibratory flap bending moments at low speed are dominated by the airloads induced by the rotor's vortex wake. A free wake model is required to predict these airloads. The free wake analysis is relatively insensitive to modeling changes including removal of bending and torsion degrees of freedom which indicates that the vibratory loads problem is essentially a forced-response problem. Improvements in prediction at low speed require improvements in modeling of the vortex wake.
4. The vibratory flap bending moments at high speed are dominated by the airloads induced by the need for roll moment balance. Details of the rotor wake in the CAMRAD/JA analysis have little effect on this airload prediction. Although modeling changes show small changes on the bending moments, they are not sufficient to explain the differences between theory and measurement seen here. More detailed flight measurements are required to identify the improvements that are needed in the analytical method.

APPENDIX 1
RESEARCH PUMA CAMRAD/JA MODEL

The research Puma was modeled in CAMRAD/JA as an isolated rotor.[2] The blade aerodynamics were modeled using 19 aerodynamic segments extending from $0.228R$ to the tip. Aerodynamic, structural, and inertial section properties were obtained from the Defence Research Agency at Farnborough. The profile of the unmodified portion of the Puma blade is a slightly modified NACA 0012 section. The chord that is added at the tip of the swept-tip blade reduces the profile thickness to a little more than 10% but it remains symmetrical. The section lift, drag, and moment values were approximated in CAMRAD/JA by using the standard NACA 0012 airfoil deck.[15] The structural properties were represented with 50 segments for both the blade modes and the inertial coefficients. The control system stiffness was chosen to match the first torsion mode inferred from flight test data obtained in stalled conditions. The tension center was assumed to be located at the quarter chord. The blade bending and torsion modes were assumed to have 0.01 structural damping, and lead-lag damping was modeled as a linear damper.

The trim solution used in CAMRAD/JA specifies the rotor lift, pitch attitude, and first harmonic flapping. The rotor lift was assumed equal to the aircraft weight for the given flight condition plus the fuselage and horizontal tail download based on wind tunnel fuselage data.[16,17] The pitch attitude was taken from a curve fit of pitch pendulum measurements with advance ratio. The CAMRAD/JA trim solution uses the blade tip flapping for its trim solution. However, the flight test measurements are for the root flapping and, to match this condition, CAMRAD/JA was run repeatedly adjusting the tip flapping targets until the correct root flapping was obtained. The measured rotor control positions are compared with the CAMRAD/JA calculated values in Figures 34 and 35 and good agreement is seen for these unspecified trim parameters using the free and prescribed wake models.

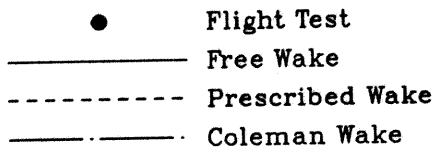

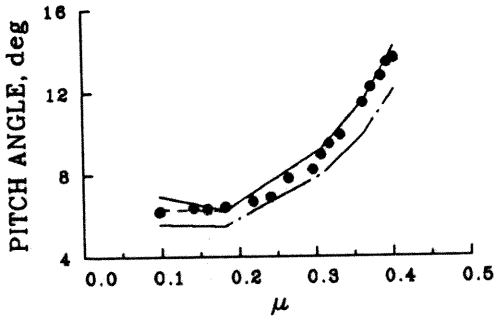

Figure 34. – Calculated and measured collective pitch for the research Puma.

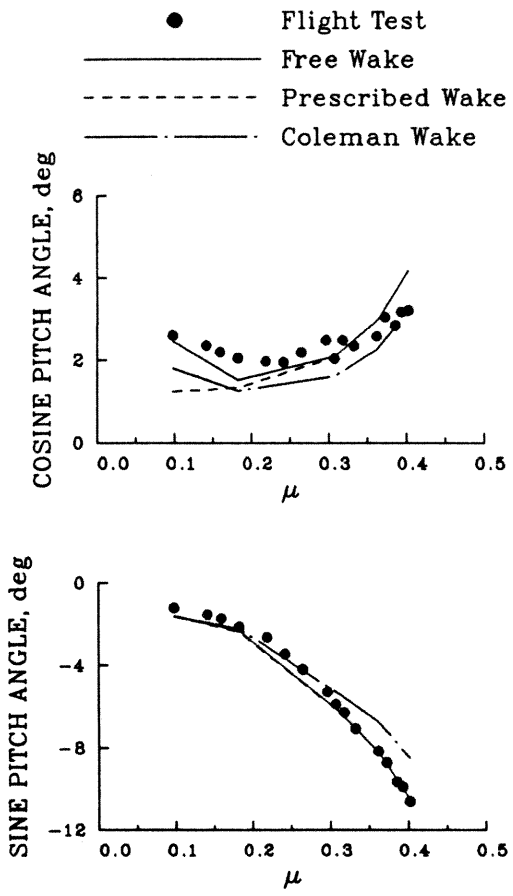

Figure 35. – Calculated and measured cyclic pitch for the research Puma.

APPENDIX 2
UH–60A CAMRAD/JA MODEL

The UH–60A was modeled in CAMRAD/JA as an aircraft with single main and tail rotors. The main rotor was modeled with 18 aerodynamic segments extending from $0.20R$ to the tip. The structure was defined by 50 segments from the centerline to the tip. Blade aerodynamic properties, such as the aerodynamic center location, chord, aerodynamic twist and so forth were obtained from Ref. 18. Slight modifications were made to these properties to account for the blade geometry defined by drawings and the trim tab effects on chord and aerodynamic center were included. Section lift, drag, and moment values for the UH–60A SC1095 and SC1094R8 airfoils were obtained from an airfoil C81 deck developed by Sikorsky Aircraft. The parameters in the wake models were identical to those used in the research Puma calculations with the exception of the core size which was scaled by the ratio of blade mean chords. Blade structural properties were obtained from Ref. 18 for the most part. The tension center was assumed to be at the blade quarter chord rather than at the blade c.g. The blade bending and torsion modes were assumed to have 0.01 structural damping. The lead-lag damper was assumed linear with the damping coefficient used in Ref. 19. Main rotor hub geometry and kinematics were determined, for the most part, from hub drawings. The control system stiffness was taken from Ref. 19.

The tail rotor was modeled with 13 aerodynamic segments outboard of $0.55R$ with the aerodynamic properties defined by Ref. 19. The SC1095 airfoil characteristics were represented by the same section properties used for the main rotor. A uniform wake model was used for all calculations. The flexbeam tail rotor was approximated as a rigid, articulated blade as the only purpose of the tail rotor in this study was to provide the correct trim forces.

The fuselage aerodynamic forces and moments were obtained from the 1/4th scale wind tunnel tests reported in Ref. 20. However, a zero angle of attack drag value of 26.2 ft^2 was used instead of the 22.0 ft^2 value obtained from the tunnel tests. The only other fuselage properties considered were the aircraft weight, c.g., and horizontal stabilator angle and these were specified to match the flight test values.

The trim solution used in CAMRAD/JA, specifies the aircraft gross weight, c.g., flight speed, and density and solves for the controls that balance the forces and moments. The sideslip angle is fixed at zero degrees and the roll angle is unspecified. The trim values were taken from the flight test measurements. The calculated shaft torque matches the measured values quite closely as shown in Figure 36. The difference is approximately $-215\ ft-lb$ which is less than 1%. The calculated rotor shaft angle of attack is compared to the measured value in Figure 37 and the agreement is reasonable at most flight speeds. The calculated tail rotor pitch angle is compared with measured values in Figure 38. The agreement is good at low speeds, but the pitch angle is overpredicted at higher speeds. Boom measurements show that the aircraft was in a nose-left sideslip at high speed for Flight 9. Calculations using the measured sideslip result in tail rotor pitch angles lower than the data shown here. Otherwise, the effect of sideslip is not apparent in the calculations.

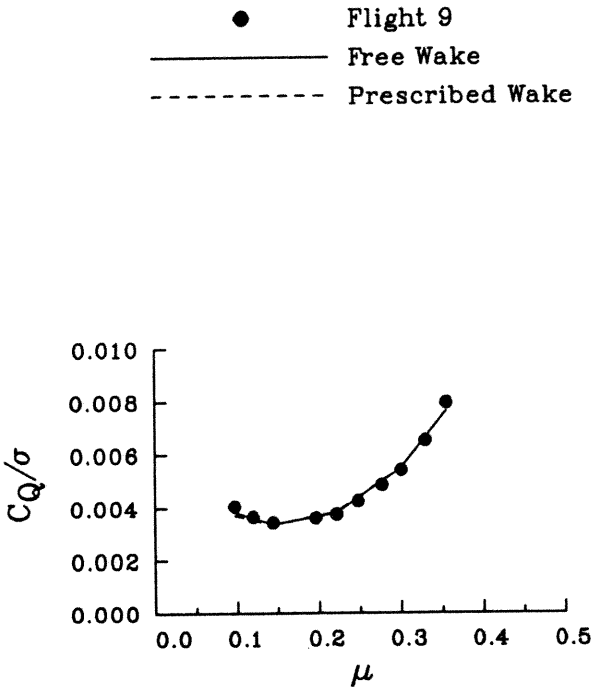

Figure 36. – Calculated and measured shaft torque for UH–60A.

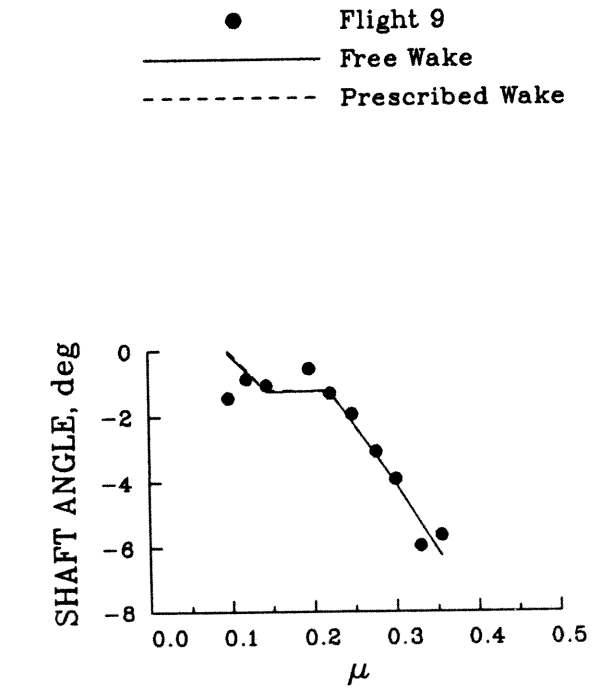

Figure 37. – Calculated and measured rotor shaft angle of attack for UH–60A.

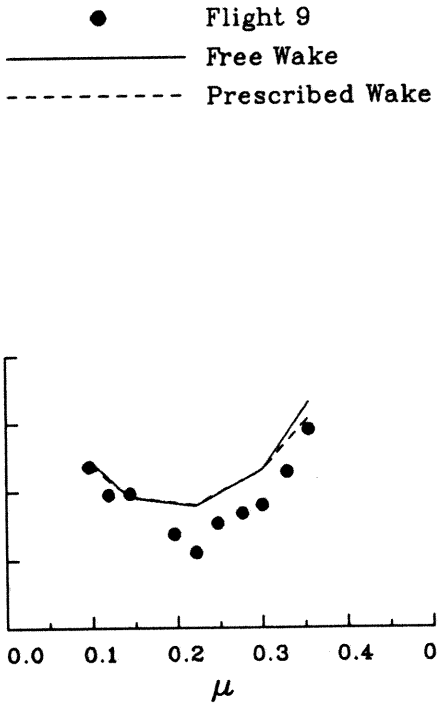

Figure 38. – Calculated and measured tail rotor pitch angle for UH–60A.

REFERENCES

[1] William G. Bousman, "The Response of Helicopter Rotors to Vibratory Airloads," *Journal of the American Helicopter Society*, Vol. 35, No. 4, October 1990, pp. 53-62.

[2] Colin Young, William G. Bousman, Thomas H. Maier, François Toulmay, and Neil Gilbert, "Lifting Line Predictions for a Swept Tip Rotor Blade," American Helicopter Society 47th Annual Forum Proceedings, May 1991, pp. 1345-1370.

[3] Wayne Johnson, "CAMRAD/JA: A Comprehensive Analytical Model of Rotorcraft Aerodynamics and Dynamics, Vol. 1, Theory Manual," Johnson Aeronautics, 1988.

[4] Robert M. Buckanin, Warren Gould, Paul W. Losier, David A. Downey, Roy Lockwood, James L. Webre, John F. Hagen, Randall W. Cason, and Christopher J. Young, "Rotor System Evaluation, Phase 1," AEFA Project No. 85-15, March 1988.

[5] Thomas H. Maier, "An Examination of Helicopter Rotor Load Calculations," American Helicopter Society National Specialists' Meeting on Rotorcraft Dynamics, November 1989.

[6] Robert M. Kufeld and Paul C. Loschke, "UH-60 Airloads Program: Status and Plans," AIAA Aircraft

Design Systems and Operations Meeting, September 1991.

[7] Jacques Esculier and William G. Bousman, "Calculated and Measured Blade Structural Response on a Full-Scale Rotor," *Journal of the American Helicopter Society*, Vol. 33, No. 1, January 1988, pp. 3-16.

[8] Karen S. Hamade and Robert M. Kufeld, "Modal Analysis of UH–60A Instrumented Rotor Blades," American Helicopter Society Specialists' Meeting: Innovations in Rotorcraft Test Technologies for the 90's, October 1990.

[9] R. A. Piziali and F. A. DuWaldt, "A Method for Computing Rotary Wing Airload Distributions in Forward Flight," U.S. Army TRECOM Report No. TR 62-44, November 1962.

[10] T. A. Egolf and A. J. Landgrebe, "Generalized Wake Geometry for a Helicopter Rotor in Forward Flight and Effect of Wake Deformation on Airloads, " American Helicopter Society 40th Annual Forum Proceedings, May 1984, pp. 359-376.

[11] Donald B. Bliss, Leo Dadone, and Daniel A. Wachspress, "Rotor Wake Modeling for High Speed Applications," American Helicopter Society 43rd Annual Forum Proceedings, May 1987, pp. 17-34.

[12] J. P. Rabbott, Jr., A. A. Lizak, and V. M. Paglino, "A Presentation of Measured and Calculated Full-Scale Rotor Blade Aerodynamic and Structural Loads," USAAVLABS TR 66-31, July 1966.

[13] Peter J. Arcidiacono and Robert Sopher, "Review of Rotor Loads Prediction Methods," AGARD-CP-334, May 1982.

[14] D. Jepson, R. Moffitt, K. Hilzinger, and J. Bissell, "Analysis and Correlation of Test Data from an Advanced Technology Rotor System," NASA CR 3714, August 1983.

[15] John M. Davis, "Rotorcraft Flight Simulation with Aeroelastic Rotor and Improved Aerodynamic Representation, Volume II – User's Manual," USAAMRDL TR 74-10B, 1974.

[16] G. Samoni, "Simulation Helicoptere Characteristic du SA 330," Aerospatiale Note Technique 330.05.0080, 1975.

[17] Padfield, G.D., "A Theoretical Model of Helicopter Flight Mechanics for Application to Piloted Simulation," RAE Technical Report No. 81048, April 1981.

[18] S. Jon Davis, "Predesign Study for a Modern 4-Bladed Rotor for the RSRA," NASA CR 166155, 1981.

[19] John P. Shanley, "Application of the Comprehensive Analytical Model of Rotorcraft Aerodynamics and Dynamics to the UH–60A Aircraft," SER-72126, February 1986.

[20] R. Barnard, "YUH–60A/T700 IR Suppressor Full Scale Prototype Test Report," SER-70094, June 1976.